ISSN 0263-2241
Volume 41
Number 2010

Measurement

ISSN 0263-2241
Volume 41
Number 2010

Measurement

Measurement

Supports *open access*

Submit your article

Menu Search in this journal

Latest issue	**Volume 219** *In progress* • 30 September 2023

About the journal

Journal of the International Measurement Confederation (IMEKO)

Contributions are invited on novel achievements in all fields of measurement and instrumentation science and technology. Authors are encouraged to submit novel material representing achievements in the field, whose ultimate goal is an enhancement of the state-of-the-art of subjects such as: ...

View full aims & scope

6.8 weeks	1.1 weeks	19%	View all insights
Review Time	Publication Time	Acceptance Rate	

Editor-in-Chief | View full Editorial Board

Professor Paolo Carbone, PhD

University of Perugia, Perugia, Italy

Articles

Latest published | Articles in press | Top cited | Most downloaded | Most popular

Research article ○ Abstract only

Study on propagation mechanism and attenuation law of acoustic emission waves for damage of prestressed steel strands

Jie Hou, ... Guangming Wu

30 September 2023

FEEDBACK

Measurement

Submit your article

Jie Yuan, ... Baiming Li
30 September 2023

Research article ○ Abstract only

Pixel-level road crack detection in UAV remote sensing images based on ARD-Unet

Yuxi Gao, ... Guoxiong Zhou
30 September 2023

Research article ● *Open access*

Metrological relations between the spray atomization parameters of a cutting fluid and formation of a surface topography and cutting force

Radosław W. Maruda, ... Grzegorz M. Królczyk
30 September 2023

View PDF

Research article ○ Abstract only

High-speed 360° 3D shape measurement based on visual stereo phase unwrapping method

Hengyu Wang, ... Bin lin
30 September 2023

Research article ○ Abstract only

Study on the electrical impedance response and conductivity mechanism of coal mass rupture under impact load

Tan Tingjiang, ... Yao Wenli
30 September 2023

Measurement

Submit your article

Research article ○ Abstract only

Data-driven model SSD-BSP for multi-target coal-gangue detection

Luyao Wang, ... Bo Li

30 September 2023

Read latest issue

Calls for papers

Special Issue on the IMEKO TC8, TC11 and TC24 2023 Conference

Guest editors: Leonardo Iannucci; Thomas Wiedenhöfer; Marija Cundeva-Blajer. Submission deadline: 15 January 2024

This Special Issue aims at collecting the extended version of the best papers presented at the IMEKO TC8, TC11 and TC24 2023 Joint Conference. This IMEKO event will be held in Madeira (Portugal) from October 11th to October 13th 2023. It is a Joint ...

Electromagnetic Measurements for Non-Destructive Metal Monitoring at Micro and Macro Scale

Guest editors: Olfa Kanoun; Sebastian Münstermann; Frank Walther; Volker Schultze; Surinder Singh.Submission deadline: 30 May 2023

Artificial Intelligence based Next Generation Optical Sensor for Sensing Application

Guest editors: Moustafa H. Aly; Amrindra Pal; Vigneswaran Dhasarathan; Kawsar Ahmed - Submission deadline: 30 May 2023

Sensors and sensor nodes are in demand around the world due to a wide range of applications in fields such as biosensing, environmental monitoring, medical field, food and safety, gas detection, temperature analysis, pressure measurement, fluid ...

View all calls for papers for special issues

Measurement

Submit your article

Approaches and current challenges in the "Measurement of Electrical Quantities" domain

Edited by Alexandru Salceanu, Luca Callegaro, Luca De Vito

3 July 2023

Artificial Intelligence based Next Generation Optical Sensor for Sensing Application

Edited by Moustafa H. Aly, Kawsar Ahmed

9 January 2023

The future glimmers long before it comes to be (TC1-TC7-TC13-TC18)

Edited by Kseniia Sapozhnikova, Eric Benoit

4 November 2022

Testing, Diagnostics & Inspection as a comprehensive value chain for Quality & Safety

Edited by Lorenzo Ciani

4 November 2022

View all special issues and article collections

View all issues

Partner journals

Measurement: Sensors

Open access

Measurement: Food

Open access

Measurement

Submit your article

For Authors

Track your accepted paper

Journal Finder

Researcher Academy

Rights and permissions

Journal Article Publishing Support Center

For Editors

Publishing Ethics Resource Kit

Guest Editors

For Reviewers

Reviewer recognition

Volume 217

August 2023

Previous vol/issue

Next vol/issue

Research article ○ Abstract only

Speed adaptive gate: A novel auxiliary branch for enhancing deep learning-based rotating machinery fault classification under varying speed conditions

Meng Rao, Ming J. Zuo, Zhigang Tian
Article 113016

Article preview

Research article ○ Abstract only

Developing a digital twin model for monitoring building structural health by combining a building information model and a real-scene 3D model

Jinghai Xu, Xin Shu, Peng Qiao, Shanshan Li, Jigang Xu
Article 112955

Article preview

Research article ○ Abstract only

An undersampling phase measurement algorithm based on parameter estimation for homodyne interferometer

Yizhou Xia, Leijie Wang, Yu Zhu, Rong Cheng, ... Liangren Xu
Article 112988

Article preview

Research article ○ Abstract only

Second-order acceleration for optical power measurement using axial thermopile detectors

Chaochen Li, Yuqiang Deng, Yunpeng Zhang, Chong Ma
Article 113006

Article preview

Research article ● *Open access*

Calibration method for fringe projection profilometry based on rational function lens distortion model

Lingbin Bu, Rong Wang, Xiaoshu Wang, Zhiwen Hou, ... Fanliang Bu
Article 112996

View PDF Article preview

Research article ○ Abstract only

Energy-saving profile optimization for underwater glider sampling: The soft actor critic method

Wenchuan Zang, Dalei Song
Article 113008

Article preview

Research article ○ Abstract only

An interpretable method for inertial platform fault diagnosis based on combination belief rule base

Manlin Chen, Zhijie Zhou, Xiaoxia Han, Zhichao Feng, You Cao
Article 112960

Article preview

Research article ○ Abstract only

Enhanced transverse nuclear magnetization of an atomic co-magnetometer at the optimal oscillating magnetic field

Zekun Wu, Gang Liu, Zhanchao Liu, Xuelei Wang, Zhen Chai
Article 113013

Article preview

Research article ○ Abstract only

Study of rail damage diagnosis and localization method based on intelligent wireless acoustic sensor network

Yin Wu, Nengfei Yang
Article 113032

Article preview

Research article ○ Abstract only

CSWGAN-GP: A new method for bearing fault diagnosis under imbalanced condition

Xi Gu, Yaoxiang Yu, Liang Guo, Hongli Gao, Ming Luo
Article 113014

Article preview

Research article ○ Abstract only

Multi-source partial discharge diagnosis in gas-insulated switchgear via zero-shot learning

Yanxin Wang, Jing Yan, Zhanbei Wang, Danchen Zhao, ... Yingsan Geng
Article 113033

Article preview

Research article ● *Open access*

Electromagnetic characteristics of 3D-printed composites by free-space measurement

Jong-Min Hyun, Jung-Ryul Lee
Article 113022

View PDF Article preview

Research article ○ Abstract only

Five-probe method for finite samples - an enhancement of the van der Pauw method

Krzysztof R. Szymański, Piotr A. Zaleski, Mirosław Kondratiuk
Article 113039

Article preview

Research article ○ Abstract only

Acoustic emission technology-based multifractal and unsupervised clustering on crack damage monitoring for low-carbon steel

Jing Huang, Zhifen Zhang, Bofang Zheng, Rui Qin, ... Xuefeng Chen
Article 113042

Article preview

Research article ○ Abstract only

Floor modal mass identification using human-induced dynamic excitation

Pengcheng Wang, Jun Chen
Article 113038

Article preview

Research article ○ Abstract only

Effects of compressed speckle image on digital image correlation for vibration measurement

Yusheng Wang, Zhixiang Huang, Pengfei Zhu, Rui Zhu, ... Dong Jiang

Article 113041

Article preview

Research article ○ Abstract only

Enhanced traffic safety and efficiency of an accelerated LC decision via DNN-APF technique

Haifeng Du, Yongjun Pan, Ibna Kawsar, Zhixiong Li, ... Adam Glowacz
Article 113029

Article preview

Research article ○ Abstract only

Pseudo label estimation based on label distribution optimization for industrial semi-supervised soft sensor

Huaiping Jin, Feihong Rao, Wangyang Yu, Bin Qian, ... Xiangguang Chen
Article 113036

Article preview

Research article ○ Abstract only

Measurement of the conductive fabric contact impedance for bioelectrical signal acquisition purposes

Ivana Kralikova, Branko Babusiak, Maros Smondrk
Article 113005

Article preview

Research article ○ Abstract only

An improved morphological transform filter for fundamental frequency phasor measurement of power system

C. Mo, T.Y. Ji, G. Mei, L.L. Zhang, Q.H. Wu
Article 113010

Article preview

Research article ○ Abstract only

Method for measuring the membrane penetration of triaxial specimens based on an external circular array of laser displacement sensors

Jiachen Zhang, Xiaomeng Ji, Xianjing Kong, Jingmao Liu, ... Yongkui Fu
Article 112905

Article preview

Research article ○ Abstract only

Optimization of the fixed-point representation of measurement data for intelligent measurement systems

Milan R. Dinčić, Zoran H. Perić, Dragan B. Denić, Bojan D. Denić
Article 113037

Article preview

Research article ○ Abstract only

A novel method for intelligent analysis of rice yield traits based on LED transmission imaging and cloud computing

Mengyu Sun, Shihao Huang, Zhihao Lu, Minghui Wang, ... Chenglong Huang
Article 113017

Article preview

Research article ○ Abstract only

FusionPID: A PID control system for the fusion of infrared and visible light images

Linlu Dong, Jun Wang
Article 113015

Article preview

Research article ○ Abstract only

Ultrasonic measurement of contact stress at metal-to-metal interface based on a real rough profile through modeling and experiment

Ting Han, Jianchun Fan
Article 113046

Article preview

Research article ○ Abstract only

Enhancing personal comfort: A machine learning approach using physiological and environmental signals measurements

Gloria Cosoli, Silvia Angela Mansi, Ilaria Pigliautile, Anna Laura Pisello, ... Marco Arnesano
Article 113047

Article preview

Short communication ○ Abstract only

Determination of propagation constant and impedance of non-reciprocal networks/lines using a generalized line-line method

Ugur Cem Hasar, Hamdullah Ozturk, Huseyin Korkmaz, Mehmet Akif Ozkaya, Omar Mustafa Ramahi
Article 113021

Article preview

Research article ○ Abstract only

Quantifying the effect of non-seasonal non-tidal loadings on background noise properties of GPS vertical displacements in mainland China

Qiwen Wu, Yuanjin Pan, Hao Ding, Yixin Xiao, Xiaoxing He
Article 113007

Article preview

Review article ○ Abstract only

A wide-angle drivable and high-precision sample goniometer for angle-resolved photoemission spectroscopy

Yoshihiro Aiura, Kenichi Ozawa, Makoto Minohara
Article 112866

Article preview

Research article ○ Abstract only

Feature extraction based on time-series topological analysis for the partial discharge pattern recognition of high-voltage power cables

Kang Sun, Rui Li, Laijun Zhao, Ziqiang Li
Article 113009

Article preview

Research article ○ Abstract only

Curvature measurement in profile bending - proposal and analysis of two application oriented measurement concepts

Thomas Kessler, Paul Winnewisser, Peter Groche
Article 112956

Article preview

Research article ○ Abstract only

Measurement and numerical analysis on dynamic performance of the LMS maglev train-track-continuous girder coupled system with running speed-up state

Dangxiong Wang, Xiaozhen Li, Chongguang Wang
Article 113052

Article preview

Research article ○ Abstract only

Real-time high-precision landslide displacement monitoring based on a GNSS CORS network

Bao Shu, Yuanhao He, Li Wang, Qin Zhang, ... Wei Qu
Article 113056

Article preview

Research article ○ Abstract only

A multi-sensor mapping Bi-LSTM model of bridge monitoring data based on spatial-temporal attention mechanism

Kang Yang, Youliang Ding, Fangfang Geng, Huachen Jiang, Zhengbo Zou
Article 113053

Article preview

Research article ○ Abstract only

A yaw correction method for pedestrian positioning using two low-cost MIMUs

Jianyu Wang, Jinhao Liu, Xiangbo Xu, Zhibin Yu, Zhe Li
Article 112992

Article preview

Research article ○ Abstract only

Research on rolling bearing fault diagnosis method based on AMVMD and convolutional neural networks

Huichao Zhang, Peiming Shi, Dongying Han, Linjie Jia
Article 113028

Article preview

Research article ○ Abstract only

Influence analysis of dynamic changes of wheel alignment parameters on high-speed rocking vibration of steering wheel

Bao Zhang, Xiaoping Su
Article 113079

Article preview

Research article ● *Open access*

500 MHz high resolution proximity sensors with fully integrated digital counter

Reza Farsi, Nergiz Sahin Solmaz, Naser Khosropour, Bruno Jacinto, ... Giovanni Boero
Article 113045

View PDF Article preview

Research article ○ Abstract only

Fault diagnosis of reciprocating machinery based on improved MEEMD-SqueezeNet

Junling Zhang, Lixiang Duan, Shilong Luo, Ke Li
Article 113026

Article preview

Research article ○ Abstract only

Fast interpolated DTFT estimators of frequency and damping factor of real-valued damped sinusoids

Daniel Belega, Dario Petri
Article 113076

Article preview

Research article ○ Abstract only

Thermal conductivity measurement of thermoelectric films using transient Photo-Electro-Thermal technique

Yifeng Ling, Meng Han, Jinqi Xie, Guojuan Qiu, ... Rong Sun
Article 113058

Article preview

Research article ○ Abstract only

Rapid texture depth detection method considering pavement deformation calibration

Hui Wang, Xun Zhang, Min Wang
Article 113024

Article preview

Research article ○ Abstract only

Impact of dynamic loading on pavement deflection measurements from traffic speed deflectometer

Kairen Shen, Hao Wang
Article 113086

Article preview

Research article ○ Abstract only

Design and optimization of a Micro-structured fiber temperature sensor based on surface plasmon resonance

Erlei Wang, Xiaodong Zhou, Honglei Yuan, Jia Li, Xiaoqing Liu
Article 113085

Article preview

Research article ○ Abstract only

A motion-blurred restoration method for surface damage detection of wind turbine blades

Ying Du, Hongkun Wu, David Garcia Cava
Article 113031

Article preview

Research article ○ Abstract only

Measurement and analysis of polarization gradient relaxation in the atomic comagnetometer

Linlin Yuan, Jiong Huang, Wenfeng Fan, Zhuo Wang, ... Wei Quan
Article 113043

Article preview

Research article ○ Abstract only

Cork classification based on multi-scale faster-RCNN with machine vision

Wenju Zhou, Yang Li, Li Liu, Haikuan Wang, Mengbo You
Article 113089

Article preview

Research article ○ Abstract only

Experimental measurement and SIR statistical analysis of wireless diversity reception over κ–μ fading channels

Danijela A. Aleksic, Aleksandar M. Kovacevic, Jelena A. Anastasov, Dejan N. Milic
Article 113048

Article preview

Research article ○ Abstract only

Noncontact measurement of tire deformation based on computer vision and Tire-Net semantic segmentation

Jie Zhang, Xuan Kong, Eugene J. OBrien, Jiaqiang Peng, Lu Deng
Article 113034

Article preview

Research article ○ Abstract only

Field measurement study on classification for mixed intense wind climate in mountainous terrain

Fanying Jiang, Jinxiang Zhang, Mingjin Zhang, Yongle Li, Jingxi Qin
Article 113064

Article preview

Research article ○ Abstract only

A rule-based modeling approach for network application availability assessment under dynamic network restoration scheme

Zhiwei Yi, Ning Huang, Qihang Yang, Xiangyu Zheng
Article 113040

Article preview

Research article ○ Abstract only

Dynamic force identification in milling based on IRLS using acceleration signals

Maxiao Hou, Hongrui Cao, Qi Li, Jianghai Shi
Article 113096

Article preview

Research article ○ Abstract only

Channel-Spatial attention convolutional neural networks trained with adaptive learning rates for surface damage detection of wind turbine blades

Zhao-Hua Liu, Qi Chen, Hua-Liang Wei, Ming-Yang Lv, Lei Chen
Article 113097

Article preview

Research article ○ Abstract only

Characterization of intersecting and bifurcating rolling contact fatigue (RCF) cracks in railway rails using ACFM sensor

Yanping Hou, Jialong Shen, Jie Fang, Zhengbing Meng, ... Lei Zhou
Article 113075

Article preview

Research article ○ Abstract only

Performance evaluation of distributed strain sensing nerves for monitoring ground collapse: A laboratory study

Yu-Xin Gao, Hong-Hu Zhu, Chao Wei, Jing Wang, Wei Zhang
Article 113100

Article preview

Research article ○ Abstract only

Measurements and estimation of frequency-dependent multi-scale viscoelastic damping properties of materials

G. Kolappan Geetha, S. Sumith, P. Angadi, D. Roy Mahapatra
Article 113093

Article preview

Research article ● *Open access*

Soft fault diagnosis in linear circuits: Test selection and non-iterative identification procedure

Stanisław Hałgas
Article 113061

View PDF Article preview

Research article ○ Abstract only

An improved prototypical network with L2 prototype correction for few-shot cross-domain fault diagnosis

Tang Tang, Jingwei Wang, Tianyuan Yang, Chuanhang Qiu, ... Liang Wang
Article 113065

Article preview

Research article ○ Abstract only

Quantifying gas emissions through vertical radial plume mapping with embedded radial basis function interpolation

Wangchun Zhang, Yujun Zhang, Ying He, Kun You, ... Boen Lei
Article 113019

Article preview

Research article ○ Abstract only

Matrix strengthening the identification of observations with split functional models in the squared $M_{split(q)}$ estimation process

Marek Hubert Zienkiewicz, Paweł S. Dąbrowski
Article 112950

Article preview

Research article ○ Abstract only

Global attention mechanism based deep learning for remaining useful life prediction of aero-engine

Zhiqiang Xu, Yujie Zhang, Jianguo Miao, Qiang Miao
Article 113098

Article preview

Research article ○ Abstract only

A high temporal-spatial resolution three-dimensional imaging method using arrayed-focus structured illumination with differential axial enhancement

Liu Zhiqun, Xue Xiaoling, Fu Lifan
Article 113063

Article preview

Research article ○ Abstract only

Cycle slip detection and repair based on the unmodeled-error-constrained geometry-free combining geometry-based models for a single-frequency receiver

Zhetao Zhang, Haijun Yuan, Xiufeng He, Jinwen Zeng
Article 113090

Article preview

Research article ○ Abstract only

How the active visual guidance device affects drivers on the foggy bridge: Safety analysis considering emergency

Yibo Dai, Yang Bian, Yiping Wu, Xiaohua Zhao, Jianhua Zhang
Article 113027

Article preview

Research article ○ Abstract only

Adaptive parameter selection variational mode decomposition based on a novel hybrid entropy and its applications in locomotive bearing diagnosis

Changjiang Xu, Jiangtian Yang, Tianyi Zhang, Kai Li, Kun Zhang
Article 113110

Article preview

Research article ○ Abstract only

Trinocular camera self-calibration based on spatio-temporal multi-layer optimization

Xin Tian, Qingji Gao, Qijun Luo, Junhu Feng
Article 113003

Article preview

Research article ○ Abstract only

Optimization of electromagnetic flow measurement system based on a new mesh electrode

Liang Ge, Sijin Wang, Ling Li, Junxian Chen, ... Xiaoting Xiao
Article 113012

Article preview

Research article ○ Abstract only

Least-squares phase-shifting algorithm of coherence scanning interferometry with windowed B-spline fitting, resampled and subdivided phase points for 3D topography metrology

Yiting Duan, Zexiao Li, Xiaodong Zhang
Article 113103

Article preview

Research article ○ Abstract only

Experimental measurement of a pulling force and determination of a friction coefficient during driven transport rollers' movement

Leopold Hrabovsky, Tomas Mlcak, Vieroslav Molnar, Gabriel Fedorko, Peter Michalik
Article 113092

Article preview

Research article ○ Abstract only

An Anti-saturation phase retrieval algorithm based on optimal composite fringe patterns for 3D measurement with shiny surface

Zhuojun Zheng, Jian Gao, Zhenyu Zheng, Lanyu Zhang
Article 113095

Article preview

Research article ○ Abstract only

Online long-distance monitoring of subway vibration reduction effect using ultra-weak fiber Bragg grating arrays

Fang Liu, Biao Xu, Honghai Wang, Jinpeng Jiang, ... Zhengying Li
Article 113057

Article preview

Research article ○ Abstract only

Circularly polarized stub-loaded annular ring patch antenna for 2×2 MIMO satellite application

Megha M. Kartha, Jayakumar M.
Article 113044

Article preview

Research article ○ Abstract only

Development of a precision vertical planar stage as a programmable planar artefact

Jiyun Zhang, Zhifeng Lou, Kuang-Chao Fan, Hanping Zhang, Jingjie Zhou
Article 113055

Article preview

Research article ○ Abstract only

Multifunctional of dual-band permittivity sensors with antenna using multicascode T-shaped resonators for simultaneous measurement of solid materials and data transfer capabilities

Syah Alam, Zahriladha Zakaria, Indra Surjati, Noor Azwan Shairi, ... Teguh Firmansyah
Article 113078

Article preview

Research article ● *Open access*

Screen-printed gold electrode for ultrasensitive voltammetric determination of the antipsychotic drug thioridazine

Jędrzej Kozak, Katarzyna Tyszczuk-Rotko
Article 113107

View PDF Article preview

Research article ○ Abstract only

An automatic exposure imaging and enhanced display method of line scan camera for X-ray defect image of solid rocket engine shell

Liangliang Li, Chuchao He, Peng Wang, Jia Ren, ... Ruohai Di
Article 113094

Article preview

Research article ○ Abstract only

Semi-supervised learning framework for crack segmentation based on contrastive learning and cross pseudo supervision

Chao Xiang, Vincent J.L. Gan, Jingjing Guo, Lu Deng
Article 113091

Article preview

Research article ○ Abstract only

Data augmentation via variational mode reconstruction and its application in few-shot fault diagnosis of rolling bearings

He Li, Zhijin Zhang, Chunlei Zhang
Article 113062

Article preview

Research article ○ Abstract only

Wireless tilt sensor based monitoring for tunnel longitudinal Settlement: Development and application

Dongming Zhang, Cong Nie, Mingqiao Chen, Hongwei Huang, Yan Wu
Article 113050

Article preview

Research article ○ Abstract only

Damage evaluation and failure mechanism analysis of axially compressed square concrete-filled steel tubular columns by acoustic emission techniques

Pan Gao, Jiepeng Liu, Xuanding Wang, Yubo Jiao, Wenchen Shan
Article 113132

Article preview

Research article ○ Abstract only

Real-time detection and analysis of foodborne pathogens via machine learning based fiber-optic Raman sensor

Bohong Zhang, Md Asad Rahman, Jinling Liu, Jie Huang, Qingbo Yang
Article 113121

Article preview

Research article ○ Abstract only

Hydraulic system fault diagnosis of the chain jacks based on multi-source data fusion

Yujia Liu, Wenhua Li, Shanying Lin, Xingkun Zhou, Yangyuan Ge
Article 113116

Article preview

Research article ○ Abstract only

Nondestructive testing of corrosion thickness in coated steel structures with THz-TDS

Xuelei Jiang, Ying Xu, Hang Hu, Wenyu Xie
Article 113088

Article preview

Research article ○ Abstract only

Gamma error correction algorithm for phase shift profilometry based on polar angle average

Bolin Cai, Chenen Tong, Qiujie Wu, Xiangcheng Chen
Article 113074

Article preview

Research article ○ Abstract only

Ultrasonic testing-based method for segmental calibration and quantitative estimation of the electrolyte content in lithium-ion batteries

Sixuan Hou, Mengchao Yi, Fachao Jiang, Languang Lu, ... Xin Lai
Article 113101

Article preview

Research article ● *Open access*

Assessing the technological quality of abrasive water jet and laser cutting processes by geometrical errors and a multiplicative indicator

Krzysztof Nadolny, Marcin Romanowski, Paweł Sutowski
Article 113060

View PDF Article preview

Review article ○ Abstract only

A review of methods for measuring oil moisture

Dongyan Zhao, Bin Zhu, Luoxin Li, Xin Liu, ... Dezhi Wu
Article 113119

Article preview

Research article ○ Abstract only

Reflection transformation calibration for mirror-assisted multi-view digital image correlation system using fluorescent speckle patterns

Kaiyu Zhu, Bing Pan
Article 113113

Article preview

Research article ○ Abstract only

Suppression of modulation-magnetic-fields crosstalk for single-beam optically-pumped magnetometers

Yuchen Suo, Xinda Song, Liwei Jiang, Le Jia, ... Zhendong Wu
Article 113059

Article preview

Research article ○ Abstract only

Generalizable end-to-end deep learning frameworks for real-time attitude estimation using 6DoF inertial measurement units

Arman Asgharpoor Golroudbari, Mohammad Hossein Sabour
Article 113105

Article preview

Research article ○ Abstract only

Numerical and experimental study on acoustic tomographic reconstruction of flow field

Qian Kong, Peng Li, Genshan Jiang, Yuechao Liu
Article 113025

Article preview

Research article ○ Abstract only

Tilted PIV: A novel approach for estimating the turbulent kinetic energy in stirred tanks

Aline G. De Mitri, Rodrigo de L. Amaral, Helder L. de Moura, Jenniffer S. Ayala, ... Guilherme J. de Castilho
Article 113112

Article preview

Research article ○ Abstract only

Highly efficient and sensitive non-enzymatic glucose biosensor based on flower-shaped CuO-colloid nanoparticles decorated with graphene-modified nanocomposite electrode

Azath Mubarakali, S. Gopinath, P. Parthasarathy, U. Arun Kumar, A. Alavudeen Basha
Article 113145

Article preview

Research article ○ Abstract only

A novel approach to using artificial intelligence in coordinate metrology including nano scale

Michal Wieczorowski, Dawid Kucharski, Pawel Sniatala, Pawel Pawlus, ... Bartosz Gapinski
Article 113051

Article preview

Research article ○ Abstract only

Thermogravimetric analysis coupled with mass spectrometry of ceramic–metal ternary composites Al_2O_3-Cu-Mo

Justyna Zygmuntowicz, Paulina Wiecińska, Marcin Wachowski, Marta Kurek, Waldemar Kaszuwara
Article 113049

Article preview

Research article ○ Abstract only

Improving RGB-D SLAM accuracy in dynamic environments based on semantic and geometric constraints

Xiqi Wang, Shunyi Zheng, Xiaohu Lin, Fengbo Zhu
Article 113084

Article preview

Page 1 of 2

Previous vol/issue

Next vol/issue

ISSN: 0263-2241

Measurement

Official Journal of the International Measurement Confederation, IMEKO

Editorial Office

Elsevier Ireland Limited, Brookvale Plaza, East Park, Shannon, Co. Clare, Ireland.
E-mail: measurement@elsevier.com

Measurement 217 (2023) 113078

Contents lists available at ScienceDirect

Measurement

journal homepage: www.elsevier.com/locate/measurement

Multifunctional of dual-band permittivity sensors with antenna using multicascode T-shaped resonators for simultaneous measurement of solid materials and data transfer capabilities

Syah Alam [a,b,*], Zahriladha Zakaria [a,*], Indra Surjati [b], Noor Azwan Shairi [a], Mudrik Alaydrus [c], Teguh Firmansyah [d]

[a] Fakulti Kejuruteraan Elektronik dan Kejuruteraan Komputer (FKEKK) of Universiti Teknikal Malaysia Melaka (UTeM), 76100 Durian Tunggal, Melaka, Malaysia
[b] Department of Electrical Engineering, Universitas Trisakti, DKI Jakarta, 11440, Indonesia
[c] Department of Electrical Engineering, Universitas Mercu Buana, DKI Jakarta, 11650, Indonesia
[d] Department of Electrical Engineering, Universitas Sultan Ageng Tirtayasa, Banten 42124, Indonesia

ARTICLE INFO

Keywords:
Antenna
Permittivity sensors
Multifunctional
Simultaneous measurement
Solid materials

ABSTRACT

This paper proposes multifunctional of a dual-band independent permittivity sensor with an antenna for data transfer capabilities. The proposed sensor consists of multicascode T-shaped resonators with single port operating at frequencies of f_{r1} = 2.45 GHz, f_{r2} = 2.00 GHz and f_{r3} = 1.50 GHz, respectively. The 1st resonant frequency was used as an antenna while the 2nd and 3rd resonant frequencies were used as sensors to determine the permittivity of solid materials simultaneously. Based on the measurement results obtained an average accuracy of 96.81% and 97.54%, while the normalized sensitivity of the proposed sensor was 0.66% and 1.77% with a permittivity range of 1 – 6.15, respectively. Furthermore, the higher resonant frequency is used as an antenna to transmit and receive data via wireless network. This research is beneficial to be applied in food, biomedical, and pharmaceutical industries to support the industry 4.0 in which the integration between sensors and the internet is required.

1. Introduction

The development of communication systems lately has been very rapid to support industry 4.0. All devices that support a system can be integrated using the internet of things [1]. One of the challenges is that a device can be integrated with other devices that can be connected wirelessly [2]. Sensors are devices that are used to detect changes in the characteristics of certain materials in specific environmental conditions [3]. One of the material characteristics that can be observed is permittivity. Material characterization is needed to detect the characteristics of materials that can be used for several applications such as the biomedical industry [4,5], the food industry [6–8], and the pharmaceutical industry [9,10]. Generally, the characterization of solid materials is carried out by observing the permittivity at a certain frequency [11,12]. Permittivity relates to the ability of a material to store an electric field under certain conditions [13]. Several approaches have been proposed to determine the permittivity of solid materials, for example using planar sensors [14,15], waveguides [1617] and combinations of active electronic components [18,19]. Planar sensors have several advantages including compact design [20], low cost, and high accuracy [21]. However, the sensor has a limited function that is to merely detect the permittivity of the material under test (MUT). In the future, multifunctional sensors are needed to be integrated with the internet-of-things and wireless-based devices and another application [22,23]. Another limitation, there is still a limited number of materials that can be characterized simultaneously. The advantage of simultaneous characterization is that there can be more than one detected material so that it can reduce the time needed to detect a large number of materials.

Generally, the previously proposed permittivity sensor [24,25] used a resonator with two ports so that it was not possible to function as an antenna simultaneously. Several previous studies have provided simultaneous material characterization solutions to determine the permittivity and thickness using microstrip line ring resonators [26], interdigital capacitors [27], and microstrip SRR structures [28].

* Corresponding authors at: Fakulti Kejuruteraan Elektronik dan Kejuruteraan Komputer (FKEKK) of Universiti Teknikal Malaysia Melaka (UTeM), 76100 Durian Tunggal, Melaka, Malaysia (S. Alam).
E-mail addresses: syah.alam@trisakti.ac.id (S. Alam), zahriladha@utem.edu.my (Z. Zakaria).

https://doi.org/10.1016/j.measurement.2023.113078
Received 25 November 2022; Received in revised form 12 April 2023; Accepted 19 May 2023
Available online 1 June 2023

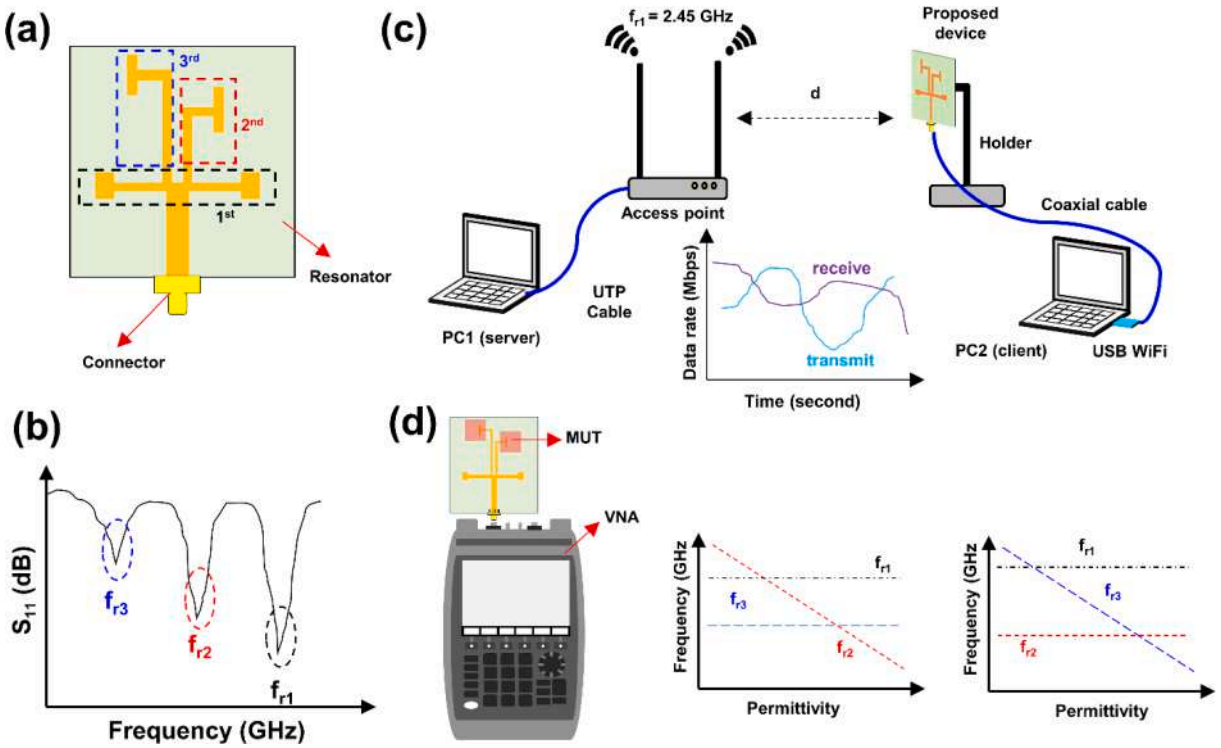

Fig. 1. (a) Structure of proposed device, (b) resonant frequency of proposed device, (c) proposed device as an antenna (d) proposed device as permittivity sensors.

Furthermore, the detection of the permittivity of solid materials was also proposed using LC resonators [29] and CSRR [30] using a dual resonant frequency approach in a single sensor structure to differentiate the permittivity of the material under test and the reference material [31]. However, the previously proposed permittivity sensor still used a resonator with two ports so it was not possible to function as an antenna and a sensor simultaneously. To produce a permittivity sensor that can also function as an antenna, a single port resonator can be used as a solution.

Previous research presented in [32] proposed the antenna as a permittivity sensor for solid materials operating at a resonant frequency of 2.5 GHz. However, the research only produced a resonator that worked at a single frequency and had one sensing hotspot, so it was not possible to determine the permittivity of two different types of MUTs simultaneously.

Another approach was carried out by [33] using a planar sensor operating at two different resonant frequencies and different sensing hotspots to detect the permittivity of solid materials independently. However, the proposed sensor could not be used as an antenna due to the poor performance of the radiation generated by the resonator. In addition, research conducted by [34] proposed a hybrid function of a dual-band resonator with an antenna where the highest resonant frequency was used as a sensor to detect the permittivity of solid materials and low frequency was used as an antenna for local transmission data. However, the previously proposed sensor only had one sensing hotspot location so it could not be used to determine the permittivity of two types of MUTs simultaneously. Furthermore, the sensor and antenna were coupled to each other so that the structure was more complex and the fabrication was complicated. Besides, the antenna and sensor were not independent of each other. Therefore, to produce a sensor that can determine permittivity simultaneously, it is necessary to have a sensor structure that operates at several different resonant frequencies, has different sensing hotspots, and has independent characteristics.

Based on literature review, typical application demanding wireless readout systems would be for a simultaneous communication-and-sensing unit for chip-less RFID sensor tags measuring temperature, humidity, and other characteristics, and communicating with a reader, at the same time [32]. Moreover, in [35] integrated microwave antenna/sensor is proposed for sensing and communication applications. The dual-functional ability of the proposed system is achieved by integrating a two-port microwave sensor and a Wi-Fi antenna with a novel frequency-selective multipath filter (FSMF). The FSMF ensures efficient system operation by not affecting the operational bandwidth of the communicating antenna in the presence of different sensed materials under test (MUTs) on top of the sensor. Furthermore, previous studied presented by [36] proposed dual-functional communication and sensing antenna system for real time detection of ice accretion in a wireless communications system (e.g., remote GPS antennas, base stations, radome of an aircraft, mobile communication systems, radio broadcasting antennas, etc.). The fixed band communicating antenna of the proposed dual-functional system is proposed for Wi-Fi application at 2.45 GHz, and the narrowband antenna sensor is used for ice/water detection.

This paper provides specific solutions to address the limitations of previous studies. The proposed sensor is multifunction device as an antenna and permittivity sensor in a single port resonator. The sensor consists of three T-shaped resonators operating at three different resonant frequencies at 2.45 GHz, 2.00 GHz, and 1.50 GHz, respectively. The proposed sensor has independent characteristics so that changes that occur in one resonator will not affect the other. Overall, the novelties and main contributions of the proposed sensor are, as follows:

1. The proposed sensor has multifunction dual-band permittivity sensor and as an antenna in a single port resonator using multicasode T-shaped.
2. The sensor operates at two different resonant frequencies and has two different locations of sensing hotspots so that it can be used to place MUTs simultaneously.
3. Furthermore, all the resonant frequencies are independent of each other so that they do not affect each other when the MUT is loaded on the resonator simultaneously.
4. The highest resonant frequency of the proposed structure is used as an antenna that functions for data transfer capabilities using the

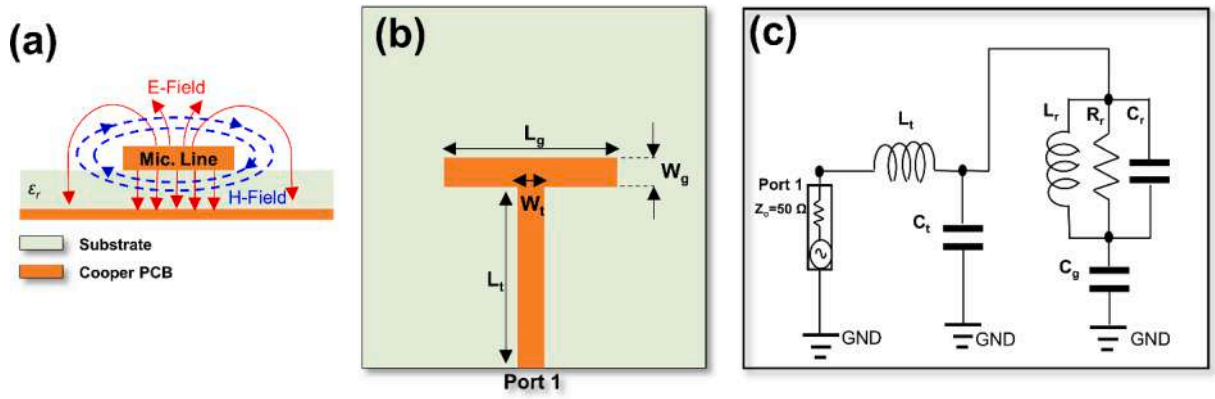

Fig. 2. (a) Physical structure of T-shaped resonators, (b) equivalent circuit of T-shaped resonators.

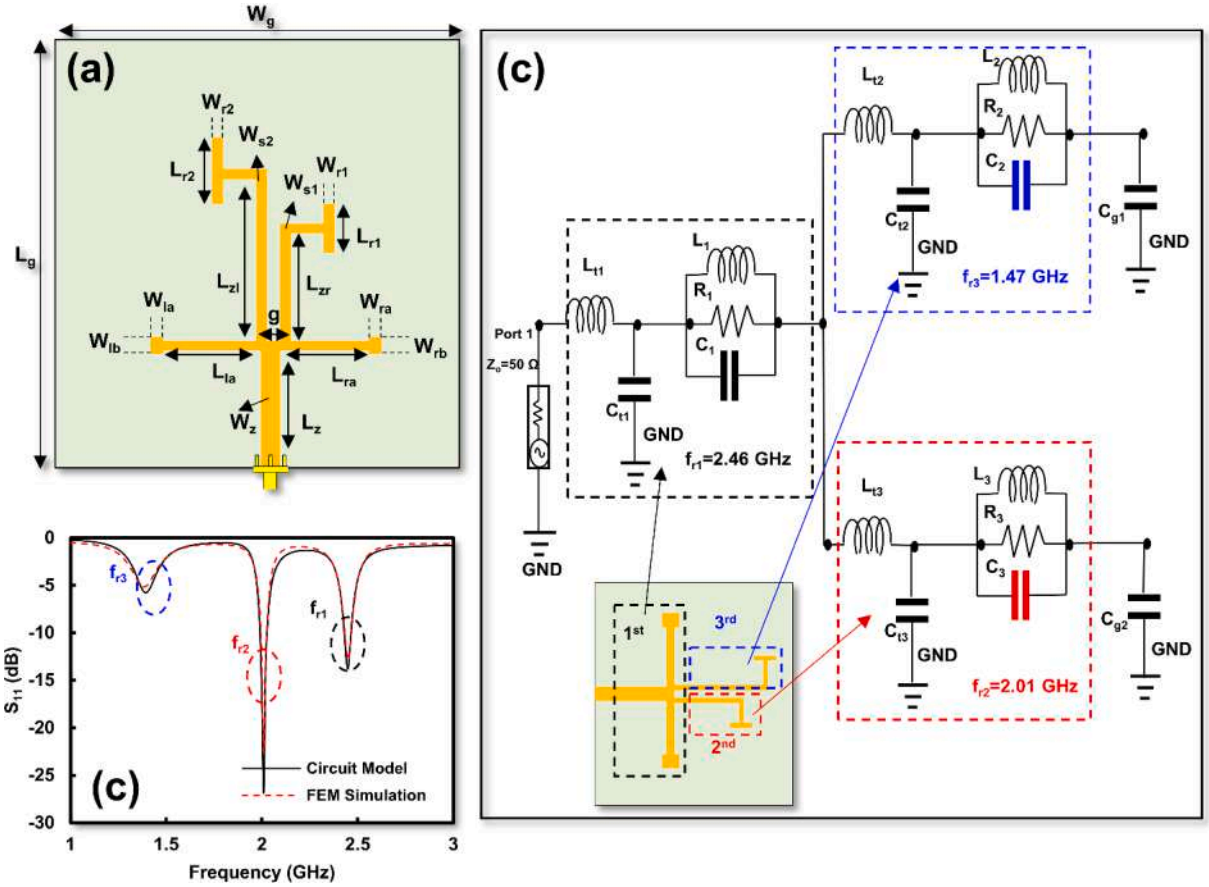

Fig. 3. (a) A proposed of multicasode T-shaped resonators design see from front view, (b) equivalent circuit of proposed resonator, (c) simulation from equivalent circuit model and Finite Element Modelling (FEM) simulation.

WLAN at 2.45 GHz while the other low frequencies are used as permittivity sensors.

This paper describes in detail starting from the working principle of the T resonator, sensor model development, equivalent circuit, simulation, and measurement of the proposed sensor. Furthermore, a mathematical model using 2nd order polynomial is proposed to determine the permittivity of the MUT. The average accuracy and normalized sensitivity are described in this paper comprehensively to evaluate the performance of the proposed sensor compared to the previously proposed sensor. The radiation pattern of the antenna at a resonant frequency of 2.45 GHz is also described to see the performance of the proposed resonator. Finally, multifunctional of dual-band permittivity sensors and antenna using multicascode T-shaped resonators can be proposed for application in the food, biomedical, and pharmaceutical industries to support industry 4.0, which requires the integration between sensors and the internet.

2. Working principle of proposed device

2.1. Working principle of a multifunctional microwave sensor with an antenna

The proposed microwave sensor operates at three different resonant

Table 1
Dimension of proposed multicascode T-shaped resonator.

Parameter	Dimension	Parameter	Dimension
L_z	15 mm	W_{la}	1 mm
W_{r1}	1 mm	W_{ra}	1 mm
L_{r1}	6 mm	W_{lb}	2 mm
W_{s1}	1 mm	W_{rb}	2 mm
W_{r2}	1 mm	L_{zr}	11.5 mm
L_{la}	15.5 mm	L_{zl}	18 mm
L_{r2}	9.5 mm	L_{ra}	13 mm
W_{s2}	1 mm	g	0.5 mm

frequencies. High frequency represented as $f_{r1} = 2.45$ GHz is used as an antenna while low frequency is represented by $f_{r2} = 2.00$ GHz and $f_{r3} = 1.50$ GHz is used as a permittivity sensor as shown in Fig. 1 (a) and Fig. 1. (b). The three resonant frequencies of the proposed device are independent so that they do not affect each other when disturbed. The permittivity sensor is used for the characterization of solid materials simultaneously at two different sensing hotspots while the antenna is used to transfer measurement data using a wireless network as shown in Fig. 1(c) and Fig. 1(d). The performance of both functions of the proposed device was observed by performing several measurements in the laboratory using supporting equipment such as vector network analyzer (VNA), access point, USB wireless and computer. The main contribution of this paper is to produce a multifunctional microwave sensor as a permittivity sensor and antenna that works for the characterization of solid materials and data transfer capabilities. In addition, the permittivity sensor has two different sensing hotspots so that it can be used to determine the permittivity of two different types of MUT simultaneously. The working principle of the proposed device is shown in Fig. 1.

The microwave sensor utilizes the electric field to determine the sensing hotspot of the sensor from the proposed device and its performance is observed from correlation of resonant frequency with permittivity of MUT obtained during the measurement process. Furthermore, the proposed device functions as an antenna by utilizing the concentration of the magnetic field from the resonator and its performance is observed from the data rates in sending and receiving data through a wireless network to send measurement data.

2.2. Working principle of T-shaped resonators

Generally, permittivity sensors utilize the capacitive characteristics of the resonator as indicated by the concentration of the electric field. The area of the resonator that has the highest electric field concentration is called the sensing hotspot. The illustration of the electric field (E-field) and magnetic field (H-field) of the microstrip line are shown in Fig. 2(a) [37]. A resonator that has capacitive characteristics will store an electric field so it can be used to determine the permittivity of the MUT. When the MUT is placed on the resonator, the electric field will create a new frequency [38]. Furthermore, the magnetic field is around the conductor of the microstrip line.

The T-shaped resonator is composed of a simple T-pattern, which includes an open-ended transmission stub and feed lines as shown in Fig. 2(b). The T-shaped resonator can be modeled with an equivalent circuit using a combination of resistor, capacitor, and inductor as shown in Fig. 2(c).

Fig. 2(b) shows the structure of a T-shaped resonator consisting of microstrip lines represented by W_t and L_t and open-ended transmission stubs represented by W_g and L_g [39]. The equivalent circuit model in Fig. 2 (c) shows that the microstrip line is represented by inductors and capacitors L_t and C_t which function as impedance-matching circuits between the resonator and port 1 while the open-ended transmission stub is represented by a combination of resistors, inductors and capacitors R_r, L_r and C_r which are all connected to ground. The width of the open-ended transmission stub of W_g represents capacitive while the length of L_g represents inductive and the resistor R_r represents tan δ of the substrate.

3. Sensors design

3.1. Structure of proposed resonator

The proposed sensor consists of three T-shaped resonators with a multicascode configuration. Each resonator operates at a different resonant frequency and is connected to port 1 using an SMA connector with an impedance of 50 Ω. The substrate used is FR-4 Epoxy with a dielectric constant (ε_r) of 4.3, a thickness (h) of 1.6 mm, and a tan δ of 0.0265. The overall dimensions of the proposed sensor are shown in Fig. 3(a) and Table 1. Fig. 3(c) shows that the 1st resonator consists of a T-shaped resonator operating at $f_{r1} = 2.46$ GHz while the 2nd and 3rd resonators operate at $f_{r2} = 2.01$ GHz and $f_{r3} = 1.47$ GHz, respectively.

Furthermore, the development equivalent circuit model of the proposed resonator shown in Fig. 3(b) consists of a combination of resistor, capacitor, and inductor. The 1st resonator represented operates at a resonant frequency of 2.46 GHz by $R_1 = 1.47$ kΩ, $L_1 = 2.65$ nH and $C_1 = 3.16$ pF while $C_{t1} = 1.06$ pF and $L_{t1} = 1.705$ nH are functioned as impedance matching circuits for high frequencies. Furthermore, the 2nd and 3rd resonators operated at resonant frequencies of 2.01 GHz and 1.47 GHz are represented by $R_3 = 0.64$ kΩ, $C_3 = 2.59$ pF, $L_3 = 1.88$ nH and $R_2 = 0.21$ kΩ, $C_2 = 2.68$ pF, $L_2 = 4.07$ nH while $C_{t3} = 0.68$ pF, $L_{t3} = 2.62$ nH, $C_{t2} = 2.42$ pF and $L_{t2} = 4.4$ nH functioned as impedance matching circuits for low frequencies, respectively. Furthermore, $C_{g1} = 1.11$ pF and $C_{g2} = 0.38$ pF are added to show that the proposed resonator is an open circuit where C_{g1} and C_{g2} show a gap between the resonator and ground plane. Fig. 3(c) shows that the simulation results of the FEM simulation are in line with the proposed equivalent circuit model. The proposed resonator between the FEM simulation and the equivalent circuit model has identical characteristics with three different resonant

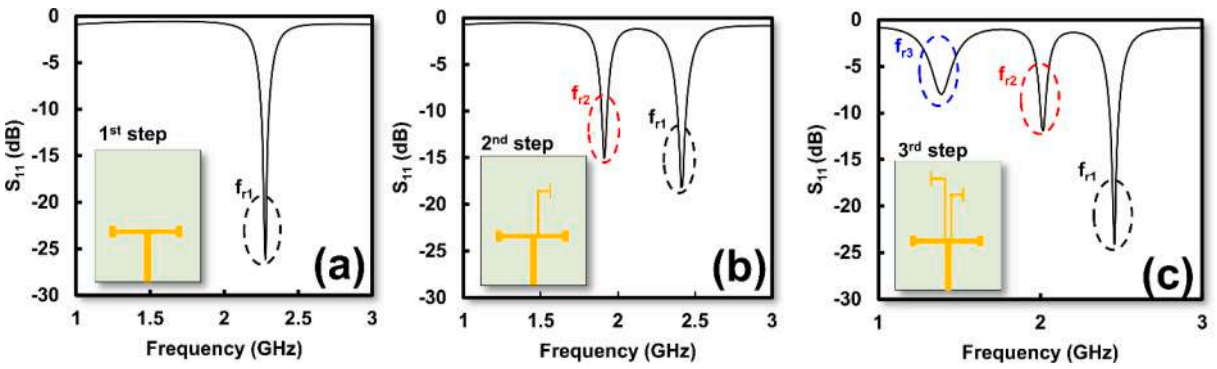

Fig. 4. (a) 1st step design of proposed resonator with single band (b) 2nd step design of proposed resonator with dual-band, (c) 3rd step design of proposed resonator with triple-band.

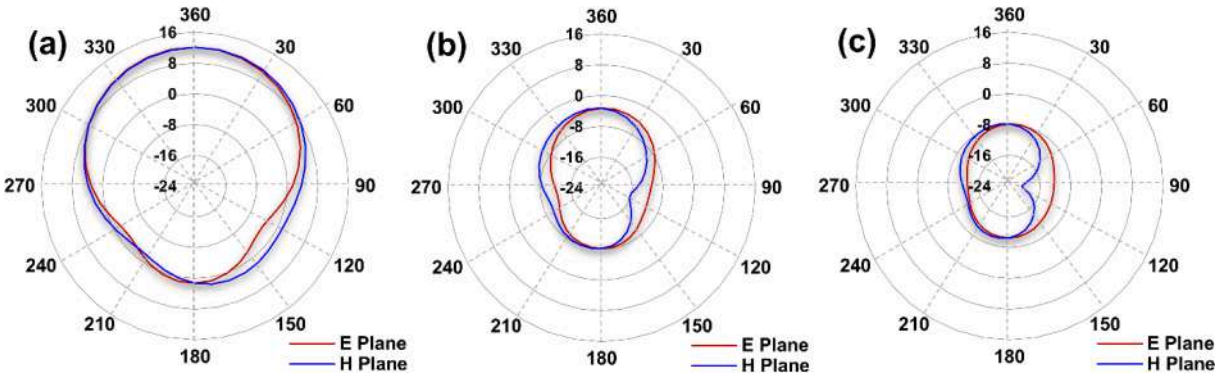

Fig. 5. Radiation pattern of proposed resonator (a) E-plane and H-Plane at $f_{r1} = 2.46$ GHz (b) E-plane and H-Plane at $f_{r2} = 2.01$ GHz, (c) E-plane and H-Plane at $f_{r3} = 1.47$ GHz.

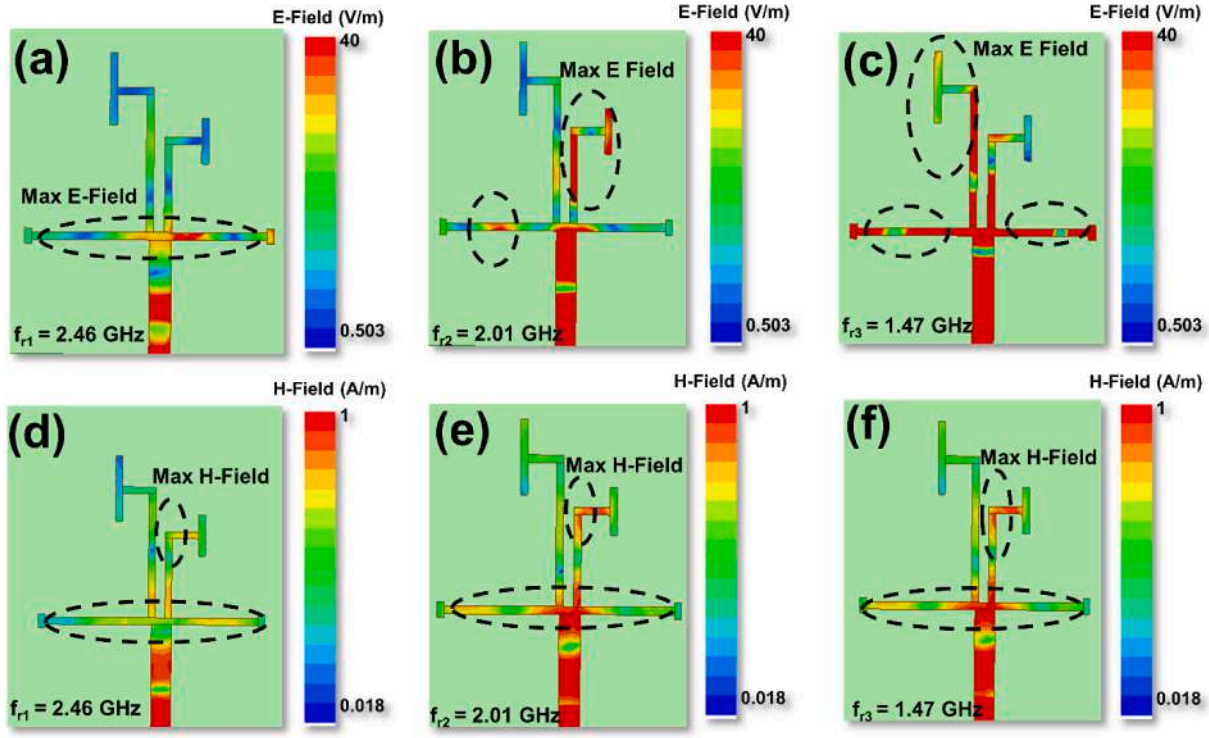

Fig. 6. E-field and H-field concentration of proposed resonator (a) E-field at $f_{r1} = 2.46$ GHz (b) E-field at $f_{r2} = 2.01$ GHz, (c) (b) E-field at $f_{r3} = 1.39$ GHz, (d) H-field at $f_{r1} = 2.46$ GHz, (e) H-field at $f_{r2} = 2.01$ GHz, (f) H-field at $f_{r3} = 1.47$ GHz.

frequencies. Based on theory, the resonant frequency of the resonator is determined from the values of L_n and C_n while R_n is used to control the value of the reflection coefficient. The frequency of each resonator will be greatly influenced by the C_{MUT} as follow [15]:

$$f_o = \frac{1}{2\pi\sqrt{L_n(C_n + C_{MUT})}} \quad (1)$$

Table 1 shows the overall dimensions of the resonators where the dimensions of the ground plane are $W_g = 50$ mm and $L_g = 50$ mm. The sensor is connected directly to a connector with an impedance of 50 Ω via a microstrip line with a width of $W_z = 3$ mm.

3.2. Development model of proposed resonator

The proposed sensor consists of three T-shaped resonators connected via microstrip lines and a connector with an impedance of 50 Ω. The development model of the resonator is shown in Fig. 4(a), Fig. 4(b), and Fig. 4(c). The 1st step model shows a T-shaped resonator design which was connected directly to the microstrip line and connector with an impedance of 50 O that operates at only one resonant frequency of 2.46 GHz. In the 2nd step model, a resonator which has an identical shape to the 1st resonator was added to produce a new resonant frequency of 2.01 GHz. Finally, in the 3rd step model, the last resonator was added which functions to produce a new resonant frequency of 1.47 GHz.

Furthermore, to observe the performance of the proposed resonator, radiation patterns of the three resonant frequencies were simulated using HFSS 15.0 as shown in Fig. 5(a), Fig. 5(b), and Fig. 5(c) where the E-plane was indicated in blue marker and H- plane with a red marker.

The simulation results showed that the resonator radiated electromagnetic waves at all three resonant frequencies as shown in Fig. 5. However, maximum electromagnetic wave radiation was only generated from the 1st resonator which operated at a resonant frequency of $f_{r1} = 2.46$ GHz with maximum radiation is 12.09 dB while that for $f_{r2} = 2.02$ GHz and $f_{r3} = 1.47$ GHz is −3.81 dB and −7.83 dB, respectively. This

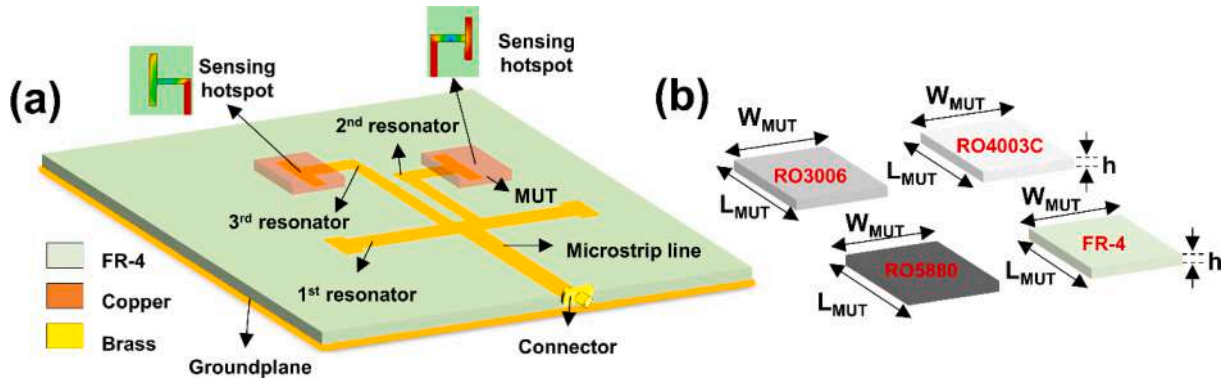

Fig. 7. (a) Placement MUT of propoposed resonator in 2nd and 3rd resonator, (b) dimensions of MUT.

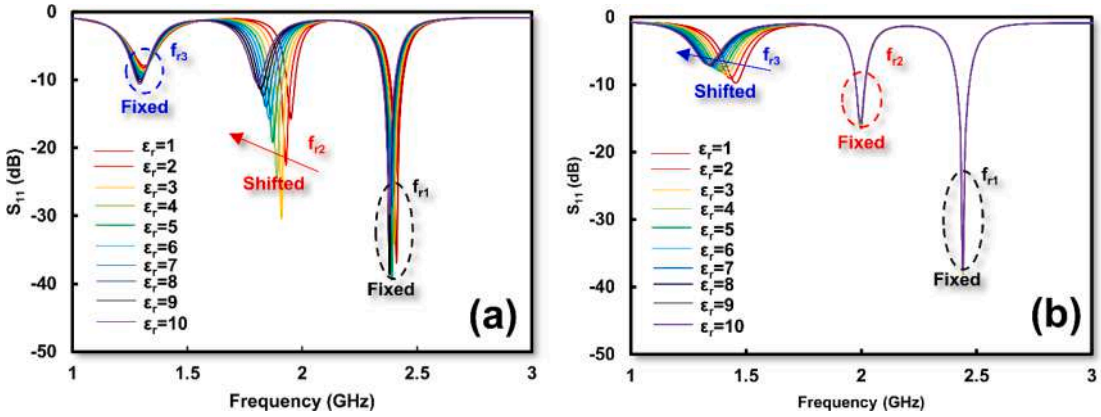

Fig. 8. Simulation of proposed resonator while MUT loaded in 2nd and 3rd resonator; (a) during scenario 1, (b) during scenario 2.

shows that the 1st resonator could be used as an antenna according to the performance of the radiation pattern obtained from the simulation results while the 2nd resonator and 3rd resonators could be used as permittivity sensors.

3.3. Placement scenario of MUT

Surface current distribution refers to the flow of electrical current that occurs on the surface of a conductive material. In the context of microwave sensors, the surface current distribution at resonant bands refers to the distribution of current that occurs on the surface of the sensor at the frequencies at which the sensor resonates. At the resonant frequency, the electromagnetic field produced by the sensor becomes highly concentrated, which causes an accumulation of charge on the surface of the sensor. This accumulation of charge results in a flow of electrical current along the surface of the sensor, which can be visualized as a distribution of current density.

In this paper, the placement location of the MUT depends on the concentration of the E-field of the resonator. Generally, the sensing hotspot is determined from the highest E-field of the resonator structure. Furthermore, the concentration of the H-field showed the characteristics of the resonator as an antenna. To determine the maximum E-field and H-field, a simulation process was carried out on the three resonant frequencies of the proposed resonator using HFSS 15.0 as shown in Fig. 6 (a), Fig. 6(b), Fig. 6(c), Fig. 6(d), Fig. 6(e), and Fig. 6(f).

Fig. 6(a) and Fig. 6(d) show the maximum E-field and H-field at $f_{r2} =$ 2.46 GHz at the same location on the arm of the 1st resonator. This showed that the 1st resonator can be used as an antenna because it has the E-field and H-Field concentrated in the same location. Furthermore, Fig. 5 (b) and Fig. 5 (e) show that the location of the maximum E-field at $f_{r2} = 2.01$ GHz is in the open-ended stub of the 2nd resonator while the maximum H-field is in the arms of the 1st and 2nd resonators. On the other hand, the location of the maximum E-field at $f_{r3} = 1.47$ GHz is on the arm and the open-ended stub of the 3rd resonator while the maximum H-field is on the arm of the 1st resonator and 2nd resonator as shown in Fig. 6 (c) and Fig. 6 (f).

Based on the simulation process and observations of the E-field and H-field concentrations of the proposed resonator, the location of the MUT is shown in Fig. 7 (a).

Fig. 7 (a) shows that the placement location of the MUT was in the open-ended stub of the 2nd and 3rd resonators while the 1st resonator was used as an antenna that functions to radiate electromagnetic waves. The MUT used is represented by W_{MUT}, L_{MUT} and h with the overall dimensions were $(10 \times 10 \times 1.6)$ mm^3 and were placed on the surface of the open-ended stubs of the 2nd and 3rd resonators as shown in Fig. 7 (b).

4. Simulation and measurement of proposed sensors

4.1. Simulation of proposed resonator using known permittivity of MUT

To determine the permittivity of the MUT, a simulation process was carried out by placing the MUT on the surface of the 2nd and 3rd resonators. The simulation used two following scenarios:

(1) The MUT was placed on the surface of the 2nd resonator while the 3rd resonator was empty (vacuum).
(2) The MUT was placed on the surface of the 3rd resonator while the 2nd resonator was empty (vacuum).

The simulation results are shown in Fig. 8 (a) and Fig. 8 (b). The permittivity range used in the simulation process was $\varepsilon_r = 1$–10 with tan

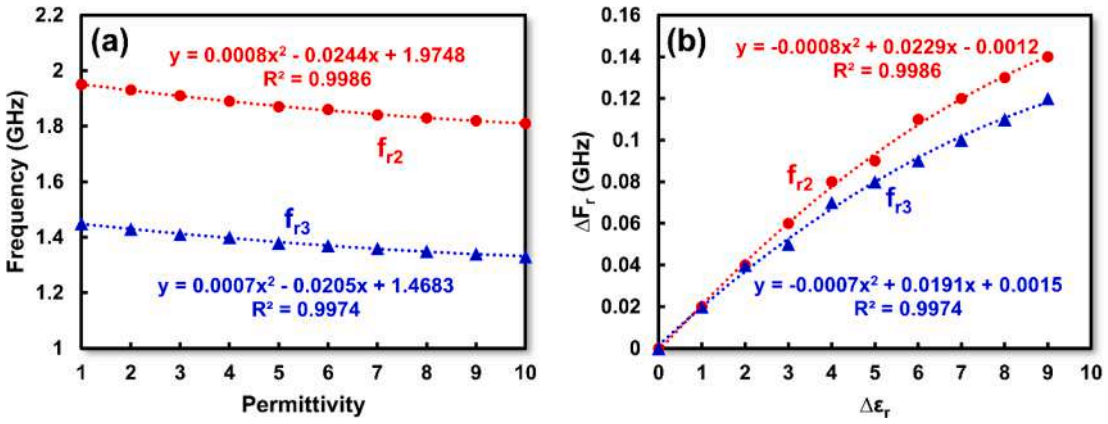

Fig. 9. (a) The effect of the change in permittivity on the resonant frequency of the resonators; (b) the maximum frequency shift (Δf_r) of the proposed sensors.

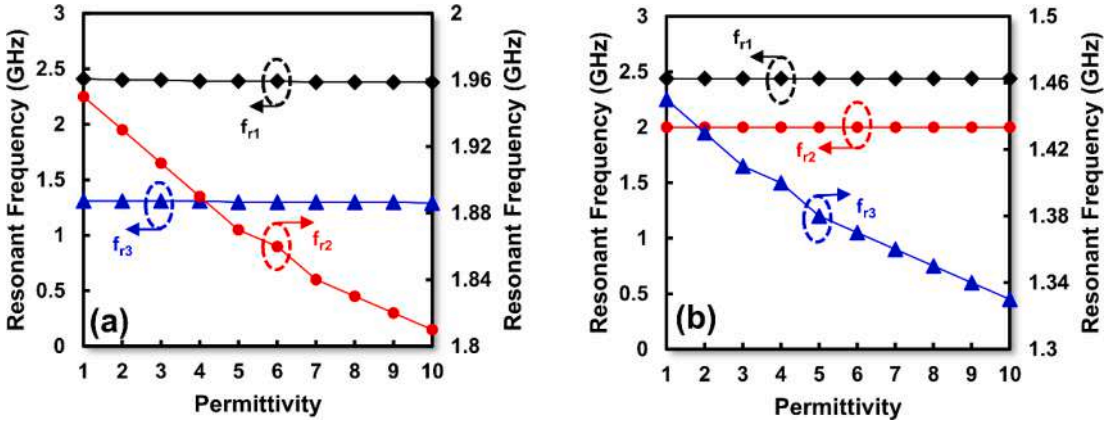

Fig. 10. Independent performance of the resonator when the permittivity changes; (a) during scenario 1, (b) during scenario 2.

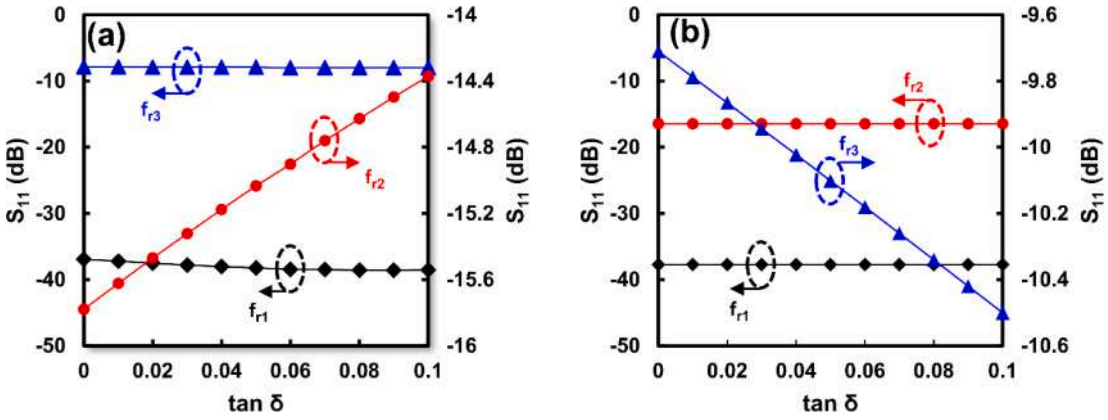

Fig. 11. The effect of the change in tan δ on the resonant frequency of resonators; (a) during scenario 1, (b) during scenario 2.

$\delta = 0$.

Fig. 8 (a) shows that in scenario (1) the resonant frequency of the 1st and 3rd resonators were fixed while the resonant frequency of the 2nd resonator shifted to a low frequency in line with the change in permittivity of the MUT. Furthermore, Fig. 8. (b) shows that in scenario (2), the frequency of the 1st and 2nd resonators was fixed while the frequency of the 3rd resonator shifted to a lower frequency in line with the change in permittivity of the MUT.

The effect of the change in permittivity of the MUT on the resonant frequencies of the 2nd and 3rd resonators during scenarios 1 and 2 is shown in Fig. 9(a) while the frequency shift is shown in Fig. 9(b). Furthermore, Fig. 9(a) shows that the resonant frequency of the 2nd resonator shifted from 1.95 GHz to 1.81 GHz while the frequency of the 3rd resonator shifts from 1.45 GHz to 1.33 GHz in line with the changes in the permittivity of the MUT from the range 1–10. Furthermore, the maximum frequency shift (Δf_r) of the 2nd resonator and 3rd resonator was 0.12 GHz and 0.14 GHz as shown in Fig. 9(b). The simulation results from scenarios (1) and (2) showed that the proposed 2nd and 3rd resonators had independent characteristics where the permittivity change only occurred when the resonator was loaded MUT at the location of the sensing hotspot as shown in Fig. 10(a) and Fig. 10(b).

In addition, the proposed sensor generated different sensing hotspot

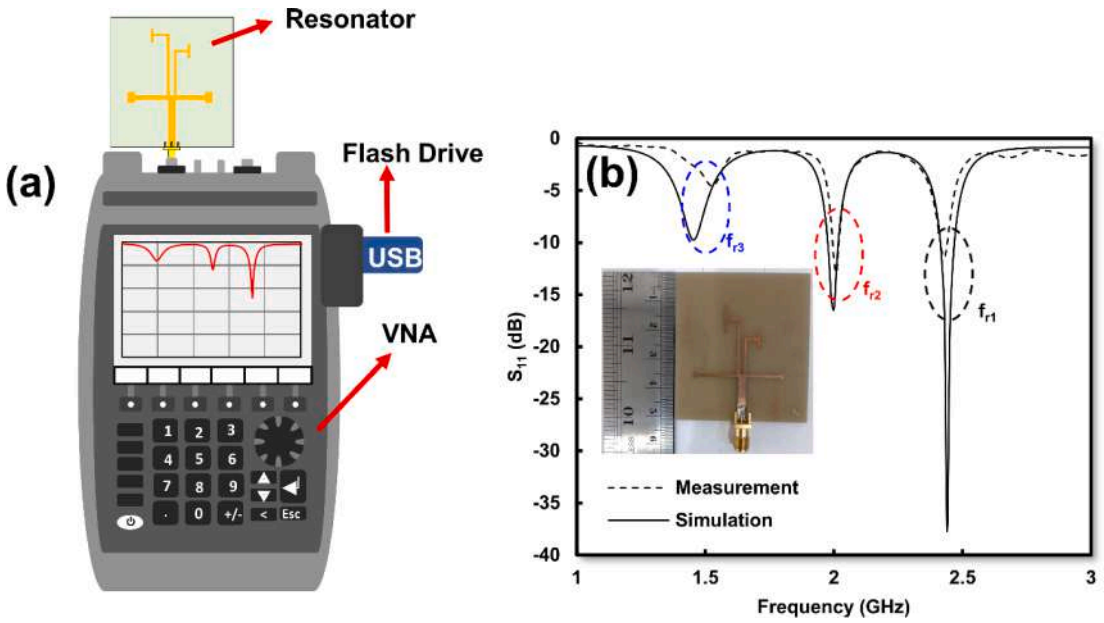

Fig. 12. (a) Measurement setup of proposed resonator, (b) simulation vs measurement result of proposed resonator.

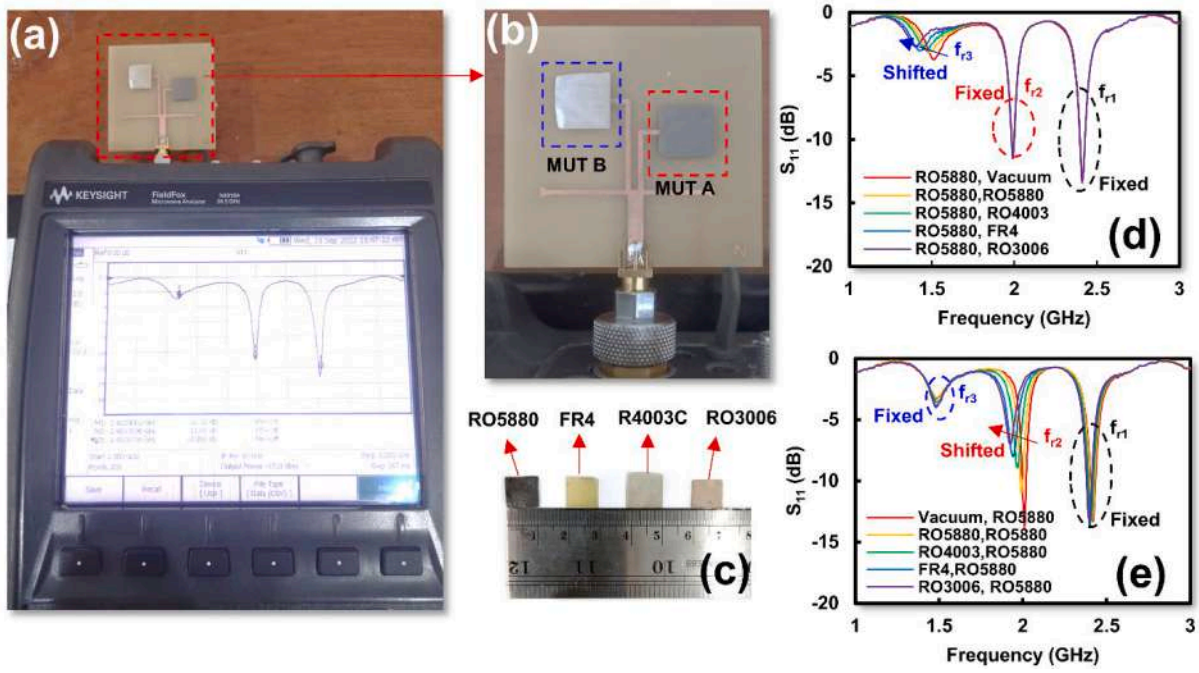

Fig. 13. (a) Measurement setup of simultaneous MUT loaded in 2nd resonator and 3rd resonator, (b) measurement result of proposed resonator during scenario 1, (c) measurement result of proposed resonator during scenario 2.

locations for the 2nd and 3rd resonators and independent characteristics of reflection coefficient when tan δ changed from 0 to 0.01 as shown in Fig. 11 (a) and Fig. 11 (b).

Fig. 11 (a) shows that the reflection coefficient of f_{r2} shifts was in line with the change in tan δ from −15.77 dB to −14.56 dB while f_{r1} and f_{r3} were fixed at −36.90 dB and −7.98 dB. Similarly, the reflection coefficient of f_{r3} shifted from −9.71 dB to −10.50 dB while f_{r1} and f_{r2} were fixed at −37.70 dB and 16.43 dB as shown in Fig. 11(b). This proves that the proposed sensor had independent characteristics based on scenarios (1) and (2). Therefore, the sensor can be used to detect the permittivity of two types of MUTs simultaneously.

4.2. Measurement process

The measurement process was carried out using a Vector Network Analyzer (VNA) which is connected directly to the proposed sensor using an SMA connector via port 1 with an impedance of 50 Ω as shown in Fig. 12(a). The frequency range used is 1.00–3.00 GHz with a sweep frequency of 0.01 GHz and an ambient temperature of 25° C. The measurement data was stored using a USB device connected to a VNA and were processed using a personal computer (PC). The comparison of the resonant frequency and reflection coefficients of the proposed resonator from the simulation and measurement process is shown in Fig. 12(b). However, there was still a slight difference between

Table 2
Characteristics and types of MUT.

Type of MUT	Parameter		
	Permittivity (ε_r)	Thickness (h)	tan δ
Vacuum	1	–	0
RO5880	2.2	1.6 mm	0.0009
RO4003	3.55	1.6 mm	0.0027
FR4	4.3	1.6 mm	0.0265
RO3006	6.15	1.6 mm	0.0025

simulation and measurement where f_{r1} shifted from 2.46 GHz to 2.45 GHz, f_{r2} from 2.01 GHz to 2 GHz, and f_{r3} from 1.47 GHz to 1.5 GHz. This was due to the variation of permittivity in the substrate, i.e., range of ε_r was 4.25 – 4.35 and also the error during the fabrication process. Overall, the errors in the measurement and simulation processes were 0.41%, 0.50% and 2.04%, respectively.

Furthermore, to observe the performance of the proposed sensor, the measurement process was carried out by placing the MUT simultaneously in each sensing hotspot. The MUT placed on the 2nd resonator was represented as MUT A while MUT B is placed on the 3rd resonator as shown in Fig. 13(a) and Fig. 13(b). The characteristics and types of MUTs used in the measurement process are shown in Table 2.

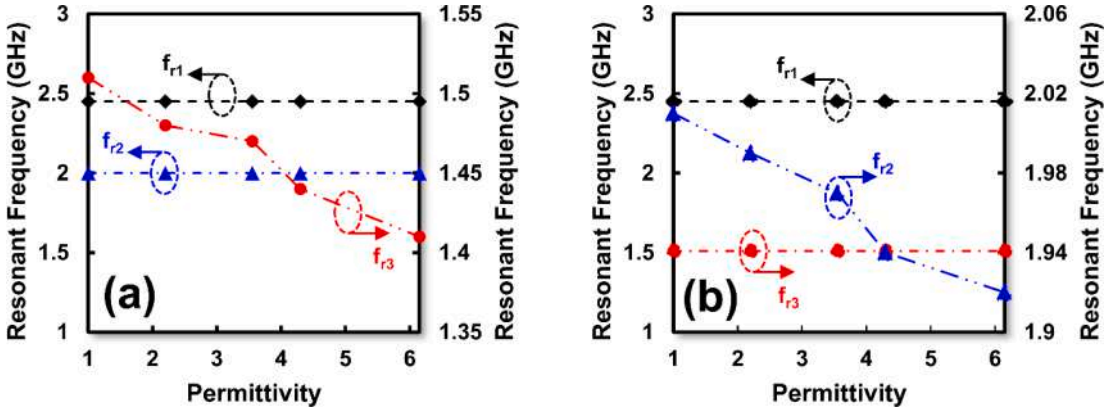

Fig. 14. (a) Correlation of f_{r1}, f_{r2} and f_{r3} at scenario 1, (b) correlation of f_{r1}, f_{r2} and f_{r3} at scenario 2.

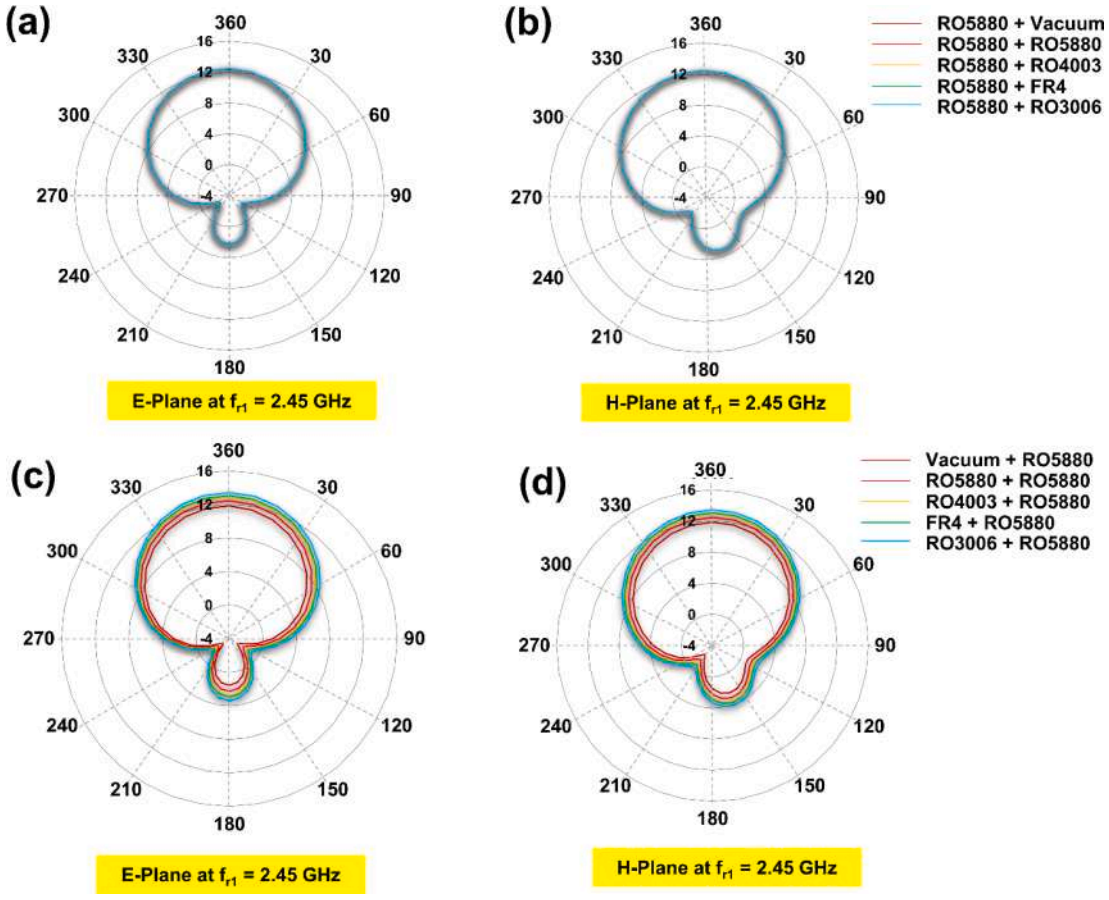

Fig. 15. (a) Radiation pattern of proposed resonator; (a) E-plane at $f_{r1} = 2.45$ during scenario 1 (b) H-plane of proposed resonator at $f_{r1} = 2.45$ GHz during scenario 1, (c) E-plane of proposed resonator at $f_{r1} = 2.45$ GHz during scenario 1, (d) H-plane of proposed resonator at $f_{r1} = 2.45$ GHz during scenario 1.

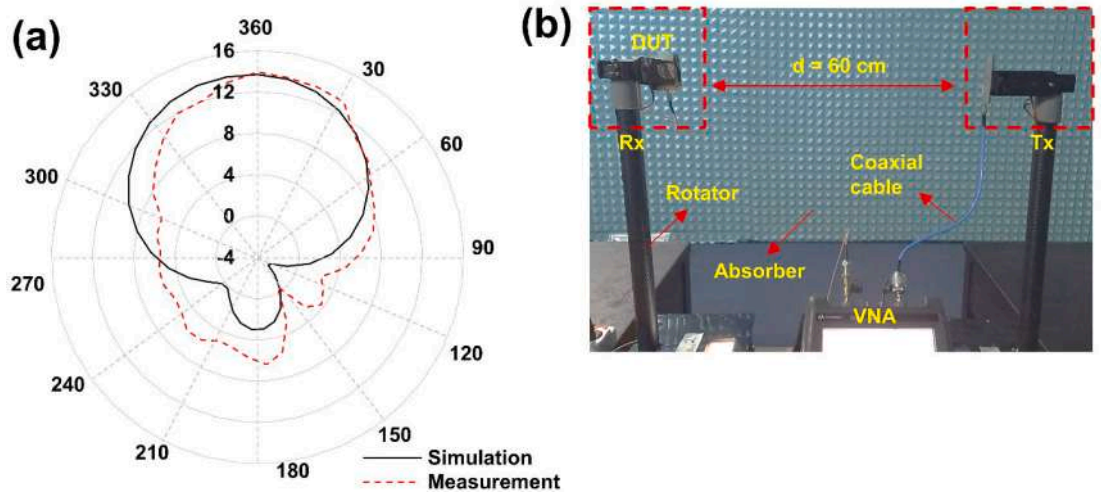

Fig. 16. (a) The radiation pattern of the antenna at $f_{r1} = 2.45$ GHz, (b) the measurement setup of the radiation pattern in the anechoic chamber.

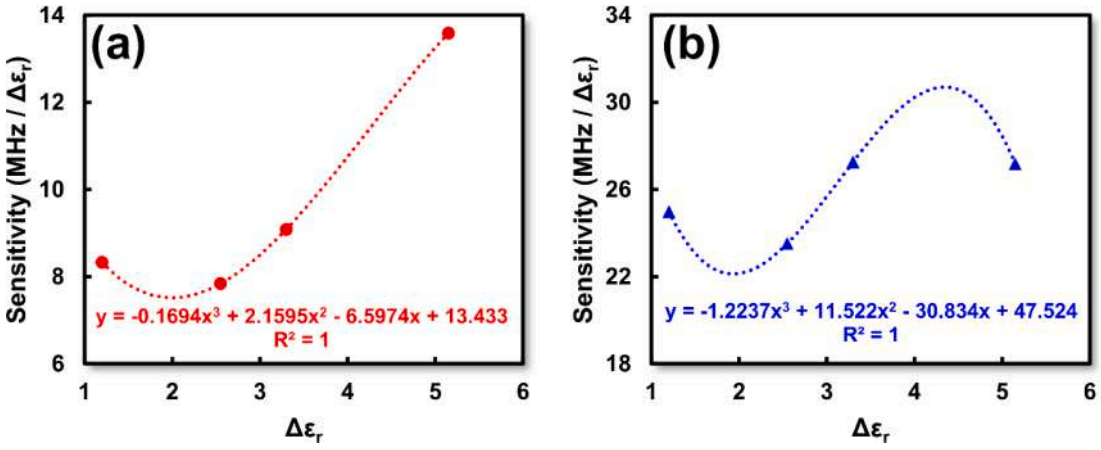

Fig. 17. (a) Sensitivity of the 2nd resonator at $f_{r2} = 2.00$ GHz, (b) sensitivity of the 3rd resonator at $f_{r3} = 1.50$ GHz.

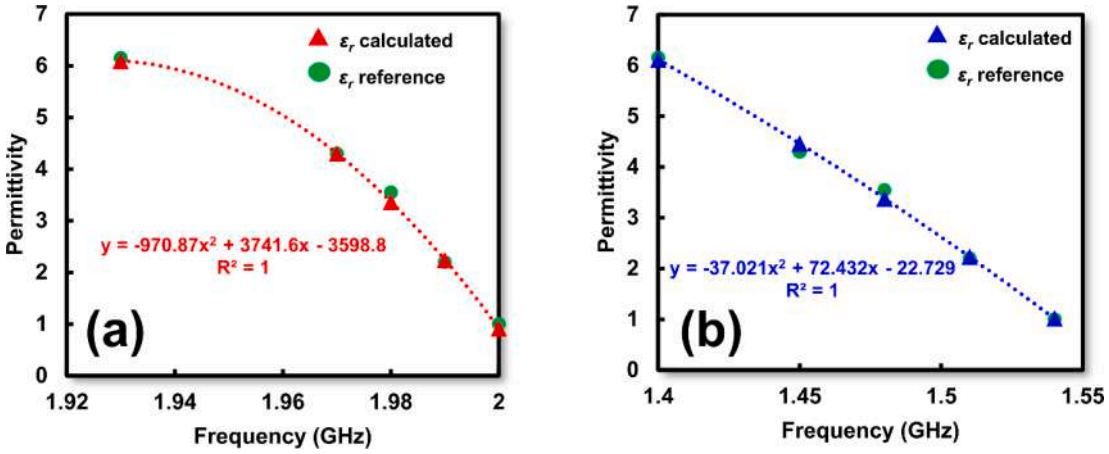

Fig. 18. (a) Accuracy of 2nd resonator compared with reference permittivity, (b) accuracy of 3rd resonator compared with reference permittivity.

The measurement process scenario used to observe the performance of the proposed sensor is as follows:

(1) MUT A placed on the 2nd resonator was fixed (RO5880) while MUT B was changed randomly.

(2) MUT B placed on the 3rd resonator was fixed (RO5880) while MUT A was changed randomly.

The dimensions of the MUT used are shown in Fig. 13 (c) which are $10 \times 10 \times 1.6$ mm^3. Furthermore, Fig. 13(d) shows that in scenario (1), f_{r3} shifted to a low frequency in line with the change in permittivity of

Table 3
Comparison of the value of the permittivity between the measurement process and the datasheet.

MUT	Parameter						
	Ref. Permittivity	Meas. Permittivity		Error (%)		Accuracy (%)	
		ε_{r1}	ε_{r2}	ε_{r1}	ε_{r2}	ε_{r1}	ε_{r2}
Vacuum	1.00	0.92	1.02	8.00	1.73	92.00	98.27
RO5880	2.20	2.24	2.23	1.89	1.44	98.11	98.56
RO4003	3.65	3.37	3.38	5.09	4.80	94.91	95.20
FR4	4.30	4.30	4.46	0.06	3.73	99.94	96.27
RO3006	6.15	6.09	6.11	0.90	0.58	99.10	99.42

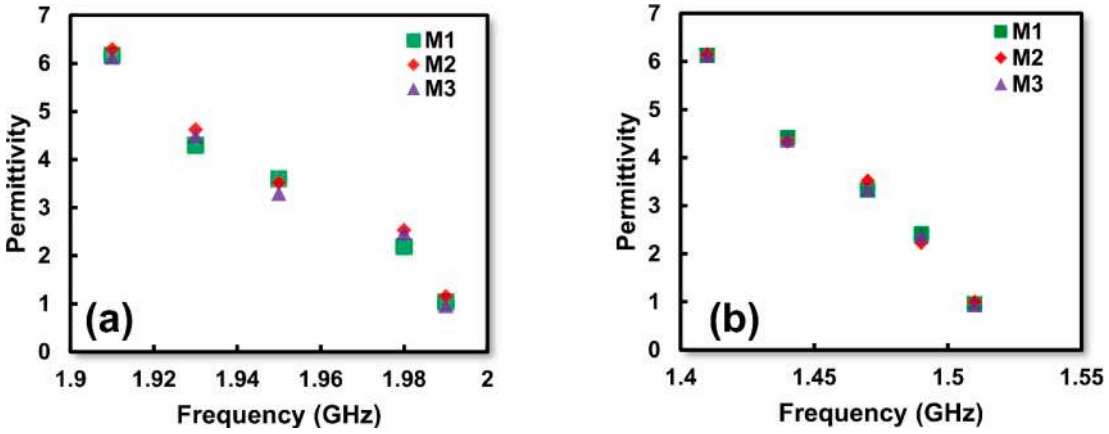

Fig. 19. Measurement of S_{11} and S_{21} from proposed resonator.

the MUT while f_{r1} and f_{r2} were fixed. Similarly, the reflection coefficients of f_{r1} and f_{r2} were also fixed because the MUT placed on the 3rd resonator is fixed (RO5880). Meanwhile, in (2), f_{r2} shifted to a low frequency in line with the change in permittivity of the MUT, while f_{r1} and f_{r3} were fixed in line with the reflection coefficient as shown in Fig. 13 (e). The correlation between each resonant frequency of the resonator to the change in the permittivity of the MUT is shown in Fig. 14(a) and Fig. 14(b).

Fig. 13(a) shows that f_{r3} shifted to a lower frequency from 1.5 GHz to 1.41 GHz while f_{r2} and f_{r1} were fixed at 2 GHz and 2.45 GHz in scenario (1). Furthermore, Fig. 13(b) shows that f_{r2} shifted to a lower frequency from 2 GHz to 1.92 GHz while f_{r1} and f_{r3} were fixed at 2.45 GHz and 1.5 GHz in scenario (2). This proves that the proposed sensor had independent characteristics and was not affected when the MUT was loaded simultaneously.

Furthermore, to observe the performance of the 1st resonator which functions as an antenna, the radiation pattern when the MUT was placed simultaneously in both sensing hotspots according to scenarios (1) and (2) are shown in Fig. 15 (a), Fig. 15 (b), Fig. 15 (c), and Fig. 15(d). The radiation pattern from the antenna during scenario 1 was fixed as shown in Fig. 15(a) and Fig. 15 (b), while Fig. 15 (c) and Fig. 15 (d) show that the radiation pattern from the antenna changed slightly in scenario (2). However, the characteristics of the radiation pattern obtained from scenario 1 and scenario (2) were still identical to each other and there was no significant change when the MUT was placed simultaneously in the sensing hotspot of the proposed sensor.

The comparison of the radiation pattern from the simulation results and the measurement process at $f_{r1} = 2.45$ GHz is shown in Fig. 16(a) while Fig. 16 (b) shows the measurement setup of the radiation pattern in the anechoic chamber. Furthermore, Fig. 16(a) shows shows that there is good agreement between the radiation patterns from the measurement and simulation results. The measurement process was carried out in the anechoic chamber where the Device Under Test (DUT) was positioned as a receiver (Rx) while the reference antenna was positioned as a transmitter (Tx) which was separated by a distance of d = 60 cm as shown in Fig. 16(b). The proposed resonator produced a directional radiation pattern with a maximum radiation of 13 dB at a resonant frequency of 2.45 GHz.

Table 4
The value of S_{11} and S_{21} of proposed resonator.

Resonator	Resonance Frequency	S_{11} (dB)	S_{21} (dB)
1st	2.45 GHz	−14.68	−26.73
2nd	2.00 GHz	−15.31	−40.65
3rd	1.50 GHz	−3.69	−52.87

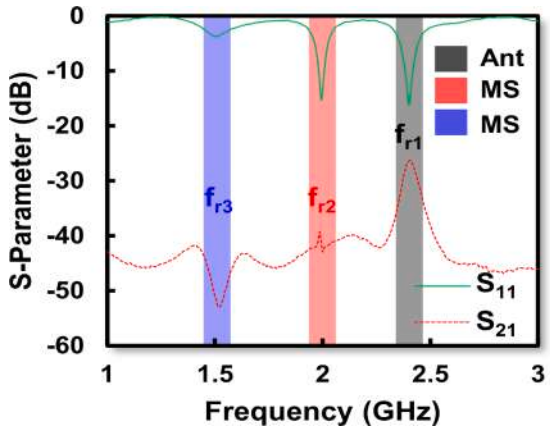

Fig. 20. Possibility scenario of permittivity detection and data transfer using proposed device.

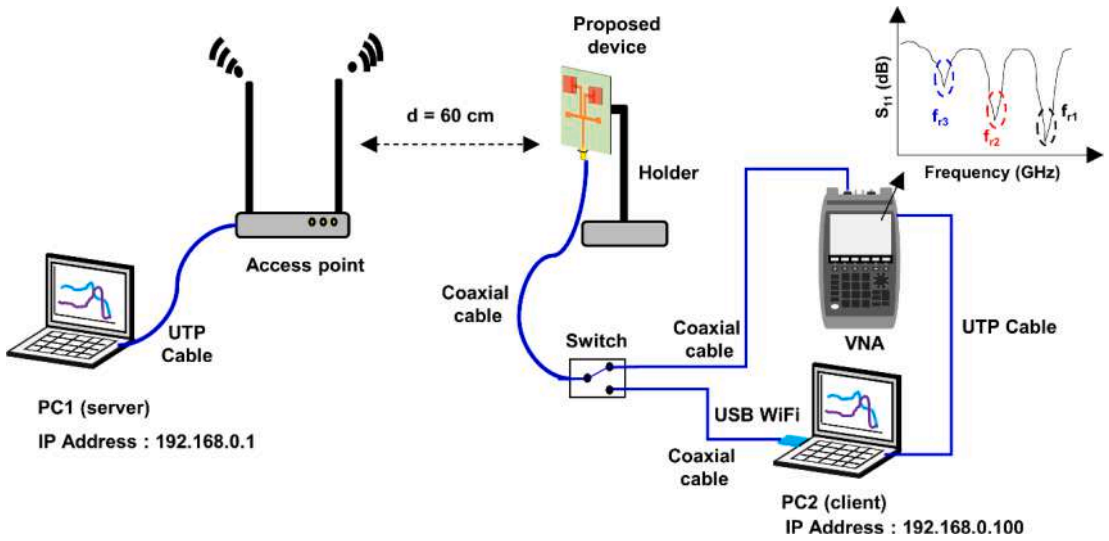

Fig. 21. Measurement setup from the proposed device for data transfer; (a) illustration of the configuration and measurement process, (b) real measurement configuration.

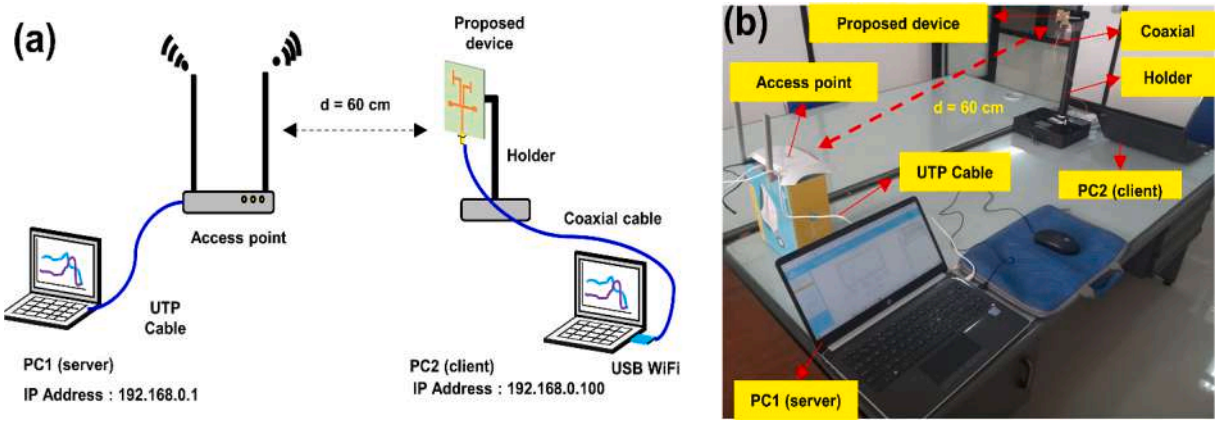

Fig. 22. Data transfer performance from the proposed device; (a) transfer data rates, (b) receive data rates.

5. Discussion

5.1. Normalized sensitivity analysis

The MUT placed in the sensing hotspot area perturbated the E-field. The interaction of the MUT to the resonator can be assumed as a capacitive load that causes the resonant frequency to shift. The ratio between the frequency shift and the change in the permittivity of the MUT was expressed as sensitivity. The sensitivity of the sensor was calculated using Eq. (2) [38]:

$$S = \frac{\Delta f}{\Delta \varepsilon_r} = \frac{(f_{unloaded} - f_{loaded})}{\varepsilon_{r(MUT)} - \varepsilon_{r(Reference)}} \tag{2}$$

Where S is the sensitivity of the sensor, Δf_r is the difference between the loaded and unloaded resonant frequency. The sensitivities of the 2nd and 3rd resonators are shown in Fig. 17(a) and Fig. 17(b). The maximum sensitivities of the 2nd resonator and 3rd resonator were 13.59 MHz/$\Delta\varepsilon_r$ and 27.27 MHz/$\Delta\varepsilon_r$, and the average sensitivities were 9.71 MHz/$\Delta\varepsilon_r$ and 25.75 MHz/$\Delta\varepsilon_r$.

Furthermore, the difference between the permittivity of the MUT and the reference is expressed as $\Delta\varepsilon_r$. Generally, the reference permittivity used is a vacuum with $\varepsilon_r = 1$ as described in [32]. The normalized sensitivity (NS) can also be calculated by Eq. (3) [25]:

$$NS = \frac{1}{\Delta \varepsilon_r}\left(\frac{f_{unloaded} - f_{loaded}}{f_{unloaded}}\right)\% \tag{3}$$

Based on Eq. (3), the normalized sensitivity (NS) of the proposed sensor was 0.68% and 1.77% with a permittivity range of 1–6.15.

5.2. Average accuracy analysis

The permittivity of the MUT was determined using a 2nd-order polynomial equation that expressed the relationship between the permittivity and the resonant frequency of the proposed sensor when the MUT was placed on the sensing hotspot as shown in Fig. 17(a) and Fig. 17(b). Furthermore, the accuracy of the sensor was obtained by comparing the calculated permittivity using a 2nd order polynomial with the reference permittivity from the datasheet.

Based on Fig. 18 (a) and Fig. 18 (b), the permittivity of the MUT was determined using the 2nd order polynomial which is expressed as follows:

$$\varepsilon_{r1} = -970.87 f_{r2}{}^2 + 3741.6 f_{r2} - 3598.8 \tag{4}$$

$$\varepsilon_{r2} = -37.021 f_{r3}{}^2 + 72.342 f_{r3} - 22.729 \tag{5}$$

The overall comparison of the permittivity between the measurement process and the datasheet is shown in Table 3.

Table 5
Comparison with sensors from previous studies.

Ref.	Model	Parameter																	
		Range of ε_r	MUT	Frequency (GHz)			Average of Accuracy (%)			NS (%)			Hybrid with antenna	Req. Cavity	Req. vias	Coupling	Layer	Sensing hotspot	Independent performance	Simultaneous measurement
				f_{r1}	f_{r2}	f_{r3}	f_{r1}	f_{r2}	f_{r3}	f_{r1}	f_{r2}	f_{r3}								
[24]	CSRR resonator	1–11.9	Solid	5.35	7.99	–	94.24	97.76	–	3.40	3.53	–	–	–	–	Direct-feed	1	1	–	–
[25]	Interdigital capasitors	1–10.5	Solid	2.51	–	–	99.40	–	–	3.98	–	–	–	–	–	Direct-feed	1	1	–	–
[26]	Microstrip line ring resonator	1–3.48	Solid	4.89	9.81	–	92.50	–	–	13.00	26.00	–	–	–	–	Direct-feed	1	1	–	–
[27]	Interdigital capasitors	1–10.2	Solid	1.50	–	–	95.30	–	–	4.40	–	–	–	–	–	Direct-feed	1	1	–	–
[28]	CSRR	1–10.2	Solid	2.4	–	–	97.79	–	–	NA	–	–	–	–	–	Direct-feed	1	1	–	–
[29]	LC resonators	1–10.2	Solid	2.00	–	–	99.90	–	–	3.28	–	–	–	–	–	Direct-feed	1	2	–	–
[30]	SRR	1–3	Solid	2.65	–	–	97.71		–	5.38	–	–	–	–	–	Direct-feed	1	1	–	–
[31]	Couple line section	1–10.2	Solid	1.50	–	–	97.50	–	–	NA	–	–	–	–	–	Direct-feed	1	1	–	–
[32]	Slot loaded	1–10.2	Solid	2.50	–	–	98.62	–	–	5.65	–	–	–	–	–	Direct-feed	1	1	–	–
[33]	U-shaped resonator	1–4.3	Solid	1.20	2.10	–	99.02	96.44	–	0.76	1.15	–	–	–	–	Direct-feed	1	2	yes	–
[34]	Apperture coupling antenna	1–12.85	Solid	9.54	12.30	–	–	92.30	–	–	0.64	–	yes	yes	yes	Magnetic	3	1	–	–
This paper	Multicascode T-shaped resonator	1–6.15	Solid	2.45	2.00	1.50	–	96.81	97.54	–	0.68	1.77	yes	–	–	Direct-feed	1	2	yes	yes

*) Req.: Required.
NS: Normalized Sensitivity.

Table 3 shows that the proposed sensor has a high accuracy in determining the permittivity of the MUT compared to the permittivity of the datasheet. The average accuracy of the proposed sensor is 96.81% and 97.54% with a permittivity range of 1–6.15.

5.3. Data transfer capability

Furthermore, to demonstrate the performance of the antenna when transmitting data, measurements of S_{11} and S_{21} are proposed as shown in Fig. 19.

Fig. 19 shows S_{11} and S_{21} of the proposed resonator when functioning as an antenna (Ant) having the same resonant frequency at $f_{r1} = 2.45$ GHz. Based on the measurement results, the magnitude of the mutual coupling (S_{21}) of the resonator increases when the resonator functions as an antenna (Ant) at $f_{r1} = 2.45$ GHz while at $f_{r2} = 2.00$ GHz and $f_{r3} = 1.50$ GHz as microwave sensor (MS) it has a lower magnitude. This shows that the resonator has functioned as an antenna at $f_{r1} = 2.45$ GHz while $f_{r2} = 2$ GHz and $f_{r3} = 1.50$ GHz can be used as permittivity sensors. Table 4 shows the value of S_{11} and S_{21} of proposed resonator for f_{r1}, f_{r2} and f_{r3}, respectively.

Moreover, to demonstrate how the permittivity data was retrieved from the wirelessly transmitted data we proposed possibility scenario of measurement process of proposed resonator as shown in Fig. 20.

Fig. 20 shows the possibility scenario of the permittivity detection process from MUT and data transfer using the proposed device. The permittivity of the MUT is detected using proposed device as microwave sensor connected to the VNA, the measurement data is stored on a PC2 which is also connected to the VNA using a UTP cable. Furthermore, to change the function of the proposed device as an antenna, a switch is proposed as a selector. Data from the measurement process is sent using the proposed device as an antenna connected to USB Wi-Fi operating at a resonant frequency of 2.45 GHz to a PC server connected to the access point. Furthermore, data transfer capability is monitored on PC1 as a server using an access point. In this paper, sensors and antennas work independently for permittivity detection and data transfer. Therefore, real-time permittivity detection using the proposed device simultaneously as sensor and antenna will be discussed as a future work. Furthermore, to observe the performance of the proposed microwave sensor as an antenna, the measurement process is performed as shown in Fig. 22 (a) and Fig. 22 (b).

Fig. 21(a) shows the configuration of the measurement process where the proposed device is connected to PC2 (client) using USB WLAN while the server located on PC1 is directly connected to an access point operating at a resonance frequency of 2.45 GHz, respectively. Furthermore, PC1 is configured as a gateway with IP address 192.168.0.1 while PC2 as a client with IP address 192.168.0.100. The distance from the server and client is represented by d = 60 cm where the client's antenna is placed in the holder and connected directly to the USB WLAN using a coaxial cable with an impedance of 50 Ohm. In addition, PC1 as a server is connected to the access point using a UTP cable as shown in Fig. 21 (b).

The performance of the proposed device is observed with the throughput monitor available on the TP Link - WR840N access point. In this experiment, the server will send measurement data to the client and vice versa via a wireless network with a file size of 150 MB. In other words, the proposed device functions as a sender and receiver of data transfer. The measurement results from the proposed device are shown in Fig. 22 (a) and Fig. 22 (b).

Fig. 22 (a) shows the maximum transfer data rates from the proposed device was 43.01 Mbps while maximum receive data rates was 41.32 Mbps as shown in Fig. 22 (b), respectively. Furthermore, the average for transfer and reception data rates was 13.32 Mbps and 26.22 Mbps. These results indicate that the proposed device has functioned as an antenna to send and receive data using a wireless network with good performance. The speed of transfer and reception data rates is greatly influenced by the quality of the signal and the size of the data packet being sent. This finding proves that the proposed microwave sensor can function as an antenna for data transfer capabilities.

5.4. Comparison with previous studied

To demonstrate the novelty and contribution of the proposed sensor, a comparison with the previously described sensors is comprehensively shown in Table 5.

Based on the comparison with previous studies, the novelty and main contribution of this research was shown by its multifunctionality as a permittivity sensor and an antenna for data transfer capabilities. In addition, the sensor had independent characteristics with two different sensing hotspots. Therefore, it can be used to detect the permittivity of two different types of MUT simultaneously. The proposed sensor had high accuracy with a compact and simple structure using a single layer thus allowing a simple measurement and easy integration with other devices.

6. Conclusion

In this paper, multifunctional dual-band microwave sensors and antenna using multicascode T-shaped resonators for simultaneous measurement of solid materials and data transfer capabilities successfully designed and implemented. The 1st resonator operating at $f_{r1} = 2.45$ GHz was used as an antenna while the 2nd and 3rd resonators operating at $f_{r2} = 2$ GHz and $f_{r3} = 1.5$ GHz were used as a permittivity sensor. The proposed sensor had independent characteristics with two different sensing hotspots so that it can be used to determine the permittivity of two different types of MUTs simultaneously. From the measurement results, the average accuracy of the proposed sensor was 96.81% and 97.54% while the normalized sensitivity (NS) was 0.68 % and 1.77% with a permittivity range of 1–6.15. Furthermore, the performance of the antenna did not change significantly when the MUT was placed simultaneously on both sensing hotspots. In addition, the proposed microwave sensor can also function as an antenna for data transfer capabilities with a average transfer and reception data rates of 13.32 Mbps and 26.22 Mbps with file size of 150 MB. The proposed sensor can be recommended as a multifunctional sensor that can be integrated with other devices via wireless for the food industry, biomedical industry, and pharmaceutical industry.

CRediT authorship contribution statement

Syah Alam: Conceptualization, Formal analysis, Methodology, Investigation, Data curation, Validation, Visualization, Writing – original draft, Writing – review & editing. **Zahriladha Zakaria:** Supervision, Resources, Writing – review & editing, Funding acquisition. **Indra Surjati:** Supervision, Resources, Writing – review & editing. **Noor Azwan Shairi:** Supervision, Resources, Writing – review & editing. **Mudrik Alaydrus:** Supervision, Resources, Writing – review & editing. **Teguh Firmansyah:** Conceptualization, Formal analysis, Data curation, Validation, Visualization, Writing – original draft, Writing – review & editing.

Declaration of Competing Interest

The authors declare that they have no known competing financial interests or personal relationships that could have appeared to influence the work reported in this paper.

Data availability

No data was used for the research described in the article.

References

[1] H. Rajab and T. Cinkelr, "IoT based Smart Cities," *2018 Int. Symp. Networks, Comput. Commun. ISNCC 2018*, no. November, pp. 1–4, 2018, doi: 10.1109/ISNCC.2018.8530997.

[2] W.A. Jabbar, et al., Design and Fabrication of Smart Home with Internet of Things Enabled Automation System, IEEE Access 7 (2019) 144059–144074, https://doi.org/10.1109/ACCESS.2019.2942846.

[3] R.A. Alahnomi, et al., Review of Recent Microwave Planar Resonator-Based Sensors, Sens. Rev. 2267 (21) (2021) 1–38.

[4] A.E. Omer, et al., Multiple-Cell Microfluidic Dielectric Resonator for Liquid Sensing Applications, IEEE Sens. J. 21 (5) (2021) 6094–6104, https://doi.org/10.1109/JSEN.2020.3041700.

[5] S. Mohammadi, R. Narang, M. Mohammadi Ashani, H. Sadabadi, A. Sanati-Nezhad, M.H. Zarifi, Real-time monitoring of Escherichia coli concentration with planar microwave resonator sensor, Microw. Opt. Technol. Lett. 61 (11) (2019) 2534–2539, https://doi.org/10.1002/mop.31913.

[6] H. Amar, H. Ghodbane, M. Amir, M.A. Zidane, C. Hamouda, A. Rouane, Microstrip sensor for product quality monitoring, J. Comput. Electron. 19 (3) (2020) 1329–1336, https://doi.org/10.1007/s10825-020-01517-2.

[7] K. Solyom, P.R. Lopez, P. Esquivel, A. Lucia, Vásquez-Caicedo,, Effect of temperature and moisture contents on dielectric properties at 2.45 GHz of fruit and vegetable processing by-products, RSC Adv. 10 (28) (2020) 16783–16790, https://doi.org/10.1039/c9ra10639a.

[8] P. Jahangiri, M. Naser-Moghadasi, B. Ghalamkari, M. Dousti, A new planar microwave sensor for fat-measuring of meat based on SRR and periodic EBG structures, Sens. Actuat. A Phys. 346 (June) (2022) 113826, https://doi.org/10.1016/j.sna.2022.113826.

[9] S.V. Kapranov, G.A. Kouzaev, Study of microwave heating of reference liquids in a coaxial waveguide reactor using the experimental, semi-analytical and numerical means, Int. J. Therm. Sci. 140 (February) (2019) 505–520, https://doi.org/10.1016/j.ijthermalsci.2019.03.023.

[10] A.A. Mohd Bahar, Z. Zakaria, M.K.M. Arshad, A.A.M. Isa, Y. Dasril, R.A. Alahnomi, Real Time Microwave Biochemical Sensor Based on Circular SIW Approach for Aqueous Dielectric Detection, Sci. Rep. 9 (1) (2019) 1–12, https://doi.org/10.1038/s41598-019-41702-3.

[11] R.A. Alahnomi, Z. Zakaria, E. Ruslan, S.R. Ab Rashid, A.A. Mohd Bahar, A. Shaaban, Microwave bio-sensor based on symmetrical split ring resonator with spurline filters for therapeutic goods detection, PLoS One 12 (9) (2017) 1–22, https://doi.org/10.1371/journal.pone.0185122.

[12] J. Muñoz-Enano, P. Vélez, M. Gil, F. Martín, Planar microwave resonant sensors: A review and recent developments, Appl. Sci. 10 (7) (2020) pp, https://doi.org/10.3390/app10072615.

[13] M.S. Boybay, O.M. Ramahi, Material characterization using complementary split-ring resonators, IEEE Trans. Instrum. Meas. 61 (11) (2012) 3039–3046, https://doi.org/10.1109/TIM.2012.2203450.

[14] A.A. Mohd Bahar, Z. Zakaria, M.K. Md Arshad, R.A. Alahnomi, A.I. Abu-Khadrah, W.Y. Sam, Microfluidic biochemical sensor based on circular SIW-DMS approach for dielectric characterization application, Int. J. RF Microw. Comput. Eng. 29 (9) (2019) 1–13, https://doi.org/10.1002/mmce.21801.

[15] A.A. Al-Behadili, I.A. Mocanu, N. Codreanu, M. Pantazica, Modified split ring resonators sensor for accurate complex permittivity measurements of solid dielectrics, Sensors (Switzerland) 20 (23) (2020) 1–18, https://doi.org/10.3390/s20236855.

[16] M. Ndoye, I. Kerroum, D. Deslandes, F. Domingue, Air-filled substrate integrated cavity resonator for humidity sensing, Sens. Actuat., B Chem. 252 (2017) 951–955, https://doi.org/10.1016/j.snb.2017.06.101.

[17] C. Sen Lee, B. Bai, Q.R. Song, Z.Q. Wang, G.F. Li, Open Complementary Split-Ring Resonator Sensor for Dropping-Based Liquid Dielectric Characterization, IEEE Sens. J. 19 (24) (2019) 11880–11890, https://doi.org/10.1109/JSEN.2019.2938184.

[18] M. Abdolrazzaghi, N. Katchinskiy, A.Y. Elezzabi, P.E. Light, M. Daneshmand, Noninvasive Glucose Sensing in Aqueous Solutions Using an Active Split-Ring Resonator, IEEE Sens. J. 21 (17) (2021) 18742–18755, https://doi.org/10.1109/JSEN.2021.3090050.

[19] M. Abdolrazzaghi, M. Daneshmand, Dual Active Resonator for Dispersion Coefficient Measurement of Asphaltene Nano-Particles, IEEE Sens. J. 17 (22) (2017) 7248–7256, https://doi.org/10.1109/JSEN.2017.2734692.

[20] M.A. Karimi, M. Arsalan, A. Shamim, Multi-Channel, Microwave-Based, Compact Printed Sensor for Simultaneous and Independent Level Measurement of Eight Liquids, IEEE Sens. J. 19 (14) (2019) 5611–5620, https://doi.org/10.1109/JSEN.2019.2904648.

[21] A.A. Abduljabar, H. Hamzah, A. Porch, Multi-resonators, microwave microfluidic sensor for liquid characterization, Microw. Opt. Technol. Lett. 63 (4) (2021) 1042–1047, https://doi.org/10.1002/mop.32675.

[22] M. Najumunnisa, et al., A Metamaterial Inspired AMC Backed Dual Band Antenna for ISM and RFID Applications, Sensors 22 (20) (2022) pp, https://doi.org/10.3390/s22208065.

[23] B. Aghoutane, S. Das, M. EL Ghzaoui, B. T. P. Madhav, and H. El Faylali, A novel dual band high gain 4-port millimeter wave MIMO antenna array for 28/37 GHz 5G applications, AEU - Int. J. Electron. Commun., vol. 145, no. August 2021, p. 154071, 2022, http://doi.org/10.1016/j.aeue.2021.154071.

[24] A. Armghan, T.M. Alanazi, A. Altaf, T. Haq, Characterization of Dielectric Substrates Using Dual Band Microwave Sensor, IEEE Access 9 (2021) 62779–62787, https://doi.org/10.1109/ACCESS.2021.3075246.

[25] C. Wang, et al., High-Accuracy Complex Permittivity Characterization of Solid Materials Using Parallel Interdigital Capacitor-Based Planar Microwave Sensor, IEEE Sens. J. 21 (5) (2021) 6083–6093, https://doi.org/10.1109/JSEN.2020.3041014.

[26] S. Lim, C.Y. Kim, S. Hong, Simultaneous Measurement of Thickness and Permittivity by Means of the Resonant Frequency Fitting of a Microstrip Line Ring Resonator, IEEE Microw. Wirel. Components Lett. 28 (6) (2018) 539–541, https://doi.org/10.1109/LMWC.2018.2833202.

[27] J. Yeo, J.I. Lee, High-sensitivity microwave sensor based on an interdigital-capacitor-shaped defected ground structure for permittivity characterization, Sensors (Switzerland) 19 (3) (2019) pp, https://doi.org/10.3390/s19030498.

[28] C. Sen Lee, C.L. Yang, Thickness and permittivity measurement in multi-layered dielectric structures using complementary split-ring resonators, IEEE Sens. J. 14 (3) (2014) 695–700, https://doi.org/10.1109/JSEN.2013.2285918.

[29] A. Ebrahimi, J. Scott, K. Ghorbani, Transmission lines terminated with LC resonators for differential permittivity sensing, IEEE Microw. Wirel. Components Lett. 28 (12) (2018) 1149–1151, https://doi.org/10.1109/LMWC.2018.2875996.

[30] M.A.H. Ansari, A.K. Jha, M.J. Akhtar, Design and Application of the CSRR-Based Planar Sensor for Noninvasive Measurement of Complex Permittivity, IEEE Sens. J. 15 (12) (2015) 7181–7189, https://doi.org/10.1109/JSEN.2015.2469683.

[31] I. Piekarz, J. Sorocki, K. Wincza, S. Gruszczynski, Microwave Sensors for Dielectric Sample Measurement Based on Coupled-Line Section, IEEE Trans. Microw. Theory Tech. 65 (5) (2017) 1615–1631, https://doi.org/10.1109/TMTT.2016.2641438.

[32] J. Yeo, J.I. Lee, Slot-loaded microstrip patch sensor antenna for high-sensitivity permittivity characterization, Electron. 8 (5) (2019), https://doi.org/10.3390/electronics8050502.

[33] S. Alam, Z. Zakaria, I. Surjati, N.A. Shairi, M. Alaydrus, T. Firmansyah, Dual-Band Independent Permittivity Sensor Using Single-Port with a Pair of U-Shaped Structures for Solid Material Detection, IEEE Sens. J. 22 (16) (2022) 16111–16119, https://doi.org/10.1109/JSEN.2022.3191345.

[34] M. Behdani, M.M.H. Kalateh, H. Saghlatoon, J. Melzer, R. Mirzavand, High-Resolution Dielectric Constant Measurement Using a Sensor Antenna with an Allocated Link for Data Transmission, IEEE Sens. J. 20 (24) (2020) 14827–14835, https://doi.org/10.1109/JSEN.2020.3012055.

[35] T. Alam, M. Cheffena, Integrated Microwave Antenna/Sensor for Sensing and Communication Applications, IEEE Trans. Microw. Theory Tech. 70 (11) (2022) 5289–5300, https://doi.org/10.1109/TMTT.2022.3199242.

[36] T. Alam, M. Cheffena, E. Rajo-Iglesias, Dual-functional communication and sensing antenna system, Sci. Rep. 12 (1) (2022) 1–11, https://doi.org/10.1038/s41598-022-24812-3.

[37] R.A. Alahnomi, Z. Zakaria, E. Ruslan, S.R. Ab Rashid, A.A. Mohd Bahar, High-Q sensor based on symmetrical split ring resonator with spurlines for solids material detection, IEEE Sens. J. 17 (9) (2017) 2766–2775, https://doi.org/10.1109/JSEN.2017.2682266.

[38] T. Haq, C. Ruan, S. Ullah, A. Kosar Fahad, Dual notch microwave sensors based on complementary metamaterial resonators, IEEE Access 7 (2019) 153489–153498, https://doi.org/10.1109/ACCESS.2019.2948868.

[39] C.L. Wu, W.H. Tu, Design of microstrip quint-band lowpass–bandpass filters with flexible passband allocation, IET Microwaves, Antennas Propag. 16 (6) (2022) 378–390, https://doi.org/10.1049/mia2.12253.

Return to Search Results

EASUREMENT

Share This Journal

SN / eISSN **0263-2241 / 1873-412X**
blisher **ELSEVIER SCI LTD, THE BOULEVARD, LANGFORD LANE, KIDLINGTON, OXFORD, ENGLAND, OXON, OX5 1GB**

eneral Information

urnal Website	Visit Site
blisher Website	Visit Site
t Year Published	1983
equency	Bi-monthly
ues Per Year	8
untry / Region	ENGLAND
imary Language	English

eb of Science Coverage

Collection	Index	Category	Similar Journals
Core Collection	Science Citation Index Expanded (SCIE)	Engineering, Multidisciplinary | Instruments & Instrumentation	Find Similar Journals
Current Contents	Electronics & Telecommunications Collection	Electronics & Electrical Engineering	Find Similar Journals
Current Contents	Engineering, Computing & Technology	Instrumentation & Measurement	Find Similar Journals
Other	Essential Science Indicators	Engineering	Find Similar Journals

arch a topic within this journal

Search a topic within this journal... Search

ournal Citation Report™ (JCR)

Journal Citation Reports™ 2022

Journal Impact Factor™ (JIF)

JCR SUBSCRIPTION NOT ACTIVE

2021	2020

Not seeing a JIF? A JCR subscription is required to view the JIF for this journal. If this is an error, please use the "Check Subscription Status" button to contact support.

Categories:
Engineering, Multidisciplinary | Instruments & Instrumentation

Not seeing a JIF? A JCR subscription is required to view the JIF for this journal. If this is an error, please use the "Check Subscription Status" button to contact support.

Categories:
Engineering, Multidisciplinary | Instruments & Instrumentation

Check Subscription Status | Learn About Journal Citation Reports™

Journal Citation Indicator (JCI) NEW METRIC

The Journal Citation Indicator is a measure of the average Category Normalized Citation Impact (CNCI) of citable items (articles & reviews) published by a journal over a recent three year period. It is used to help you evaluate journals based on other metrics besides the Journal Impact Factor (JIF).

2021	2020
1.52	1.38
Categories: Engineering, Multidisciplinary | Instruments & Instrumentation	**Categories:** Engineering, Multidisciplinary | Instruments & Instrumentation

Learn About Journal Citation Indicator

eer Review Information

pe of Peer Review	Single blind
eb of Science Reviewer Recognition	No
aimed Reviews on Web of Science	8,310
blic Reports on Web of Science	No
gned Reports on Web of Science	No
ansparent Peer Review on ScholarOne	No
ports Published	No
thor Responses to Reviews Published	No
itorial Decision Letters Published	No
evious Versions of Manuscript Published	No
viewer Identities Published	No
viewer Identities Revealed to Author	No
blic Commenting	No
viewers Consult with Each Other	No

Create a free *Web of Science profile* to track your publications, citation metrics, peer reviews, and editing work for this journal.

ubMed® Information

dexed In	PubMed®
M® ID	101668765
rporate Author	International Measurement Confederation.|Institute of Measurement and Control.

Courtesy of the U.S. National Library of Medicine

Alam, Syah

Universitas Trisakti, Jakarta, Indonesia 57191903622 https://orcid.org/0000-0002-0162-8364

138	43	7
Citations by ***96 documents***	Documents	*h*-index View *h*-graph

Set alert Edit profile ••• More

Document & citation trends

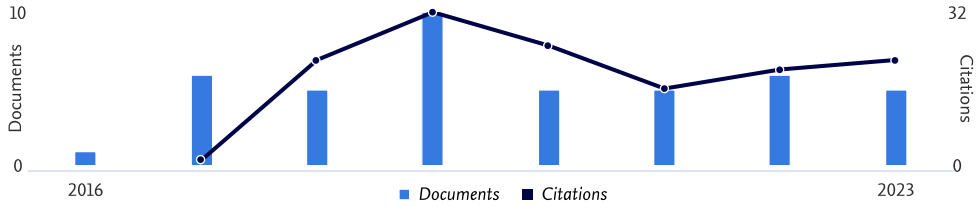

Scopus Preview

Scopus Preview users can only view a limited set of features. Check your institution's access to view all documents and features.

Check access

43 Documents Cited by 96 documents 1 Preprint 55 Co-Authors 0 Topics Awarded Grants Beta

Note:

Scopus Preview users can only view an author's last 10 documents, while most other features are disabled. Do you have access through your institution? Check your institution's access to view all documents and features.

43 documents

Export all Save all to list Sort by Date (...

Article

Modeling of quasi-tapered microstrip antenna based on expansion-exponential tapered method and its application for wideband MIMO structure

0 Citations

Firmansyah, T., Praptodiyono, S., Permana, J., ...Alaydrus, M., Kondoh, J.

AEU - International Journal of Electronics and Communications, 2023, 169, 154745

Show abstract Related documents

Article

Multifunctional of dual-band permittivity sensors with antenna using multicascode T-shaped resonators for simultaneous measurement of solid materials and data transfer capabilities

0 Citations

Alam, S., Zakaria, Z., Surjati, I., ...Alaydrus, M., Firmansyah, T.

Measurement: Journal of the International Measurement Confederation, 2023, 217, 113078

Show abstract Related documents

Article

Integrated Microwave Sensor and Antenna Sensor Based on Dual T-Shaped Resonator Structures for Contact and Noncontact Characterization of Solid Material

0 Citations

Alam, S., Zakaria, Z., Surjati, I., ...Alaydrus, M., Firmansyah, T.

IEEE Sensors Journal, 2023, 23(12), pp. 13010–13018

Show abstract Related documents

Review • *Open access*

A Compact and Low-Profile Curve-Feed Complementary Split-Ring Resonator Microwave Sensor for Solid Material Detection

3 Citations

Al-Gburi, A.J.A., Zakaria, Z., Abd Rahman, N., Alam, S., Said, M.A.M.

Micromachines, 2023, 14(2), 384

Show abstract Related documents

Conference Paper

Highly Independent Dual-Band Permittivity Sensors for Simultaneous Measurement of Solid Materials

0 Citations

Alam, S., Zakaria, Z., Surjati, I., ...Alaydrus, M., Firmansyah, T.

2023 33rd International Conference Radioelektronika, RADIOELEKTRONIKA 2023, 2023

Show abstract Related documents

Article • *Open access*

Bandwidth Enhancement of Bow-tie Microstrip Patch Antenna Using Defected Ground Structure for 5G

2 Citations

Astuti, D.W., Fadilah, R., Muslim, ...Alam, S., Wahyu, Y.

Journal of Communications, 2022, 17(12), pp. 995–1002

Show abstract Related documents

Article

Dual-Band Independent Permittivity Sensor Using Single-Port with a Pair of U-Shaped Structures for Solid Material Detection

9 Citations

Alam, S., Zakaria, Z., Surjati, I., ...Alaydrus, M., Firmansyah, T.

IEEE Sensors Journal, 2022, 22(16), pp. 16111–16119

Show abstract Related documents

Article

POLAR CODE PERFORMANCE ANALYSIS FOR HIGH-SPEED WIRELESS DATA COMMUNICATION SYSTEM

0 Citations

Sari, L., Gultom, Y.K., Alam, S., Surjati, I.

Journal of Theoretical and Applied Information Technology, 2022, 100(7), pp. 1974–1982

Show abstract Related documents

Article • *Open access*

Solid Characterization Utilizing Planar Microwave Resonator Sensor

4 Citations

Al-Gburi, A.J.A., Zakaria, Z., Ibrahim, I.M., Aswir, R.S., Alam, S.

Applied Computational Electromagnetics Society Journal, 2022, 37(2), pp. 222–228

Show abstract Related documents

Article • *Open access*

Bandwidth Enhancement and Circular Polarization Microstrip Antenna Using L Slot and Rectangular Parasitic Stacked | Мікросмужкова антена з розширенням смуги пропускання та круговою поляризацією з використанням L-слоту та стопкою прямокутних паразитних елементів

0 Citations

Alam, S., Surjati, I., Sari, L., ...Zakaria, Z., Shairi, N.A.

Journal of Nano- and Electronic Physics, 2022, 14(4), 04029

Show abstract Related documents

Back to top

Author Position

Based on 38 documents for 2013 - 2022

First author 53%

20	3	0.814
Documents	Average citations	Average FWCI

Last author 21%

Co-author 26%

Corresponding author 21%

Single author 0%

View author position details

View list in search results format

View references

Set document alert

About Scopus

What is Scopus

Content coverage

Scopus blog

Scopus API

Privacy matters

Language

日本語版を表示する

查看简体中文版本

查看繁體中文版本

Просмотр версии на русском языке

Customer Service

Help

Tutorials

Contact us

ELSEVIER

Measurement: Journal of the International Measurement Confederation

COUNTRY

Netherlands

Universities and research institutions in Netherlands

Media Ranking in Netherlands

SUBJECT AREA AND CATEGORY

Engineering
- Electrical and Electronic Engineering

Mathematics
- Applied Mathematics
- Statistics and Probability

Physics and Astronomy
- Condensed Matter Physics
- Instrumentation

Social Sciences
- Education

PUBLISHER

Elsevier

H-INDEX

115

PUBLICATION TYPE

Journals

ISSN

02632241

COVERAGE

1983-2022

INFORMATION

Homepage

How to publish in this journal

measurement@elsevier.com

SCOPE

Contributions are invited on novel achievements in all fields of measurement and instrumentation science and technology. Authors are encouraged to submit novel material, whose ultimate goal is an advancement in the state of the art of: measurement and metrology fundamentals, sensors, measurement instruments, measurement and estimation techniques, measurement data processing and fusion algorithms, evaluation procedures and methodologies for plants and industrial processes, performance analysis of systems, processes and algorithms, mathematical models for measurement-oriented purposes, distributed measurement systems in a connected world.

Join the conversation about this journal

Quartiles

FIND SIMILAR JOURNALS options

1	2	3	4	5
Metrology and Measurement Systems	Journal of Vibroengineering	Measurement and Control	Shock and Vibration	Frontiers of Mechanical Engineering
POL	LTU	USA	EGY	CHN
34% similarity	30% similarity	29% similarity	24% similarity	24% similarity

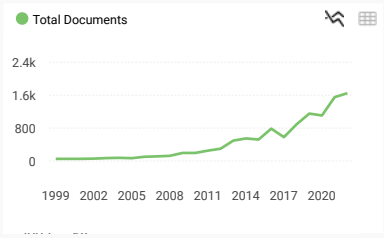

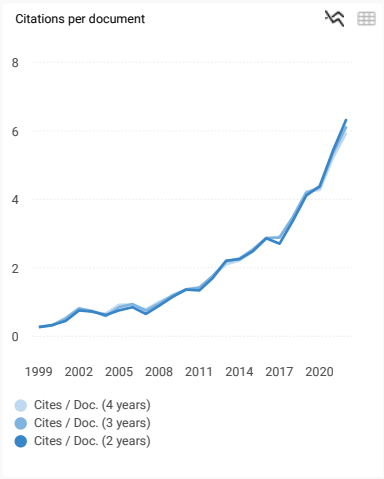

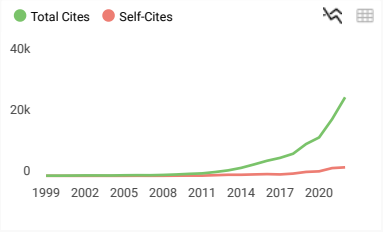

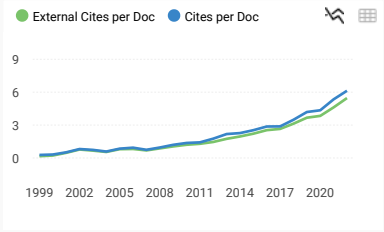

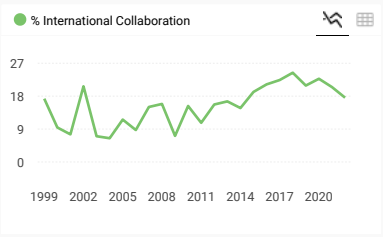

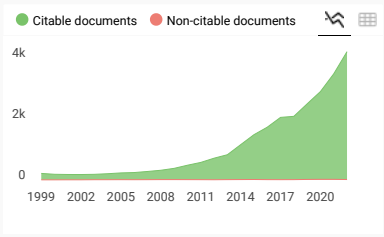

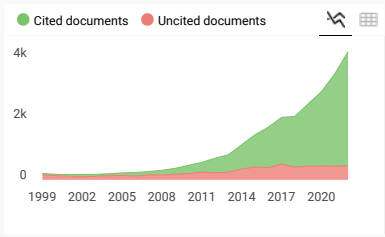

← Show this widget in your own website

Just copy the code below and paste within your html code:

<a href="https://www.scimag

SCImago Graphica

Explore, visually communicate and make sense of data with our **new data visualization tool**.

Metrics based on Scopus® data as of April 2023

Loading comments...

Developed by: SCImago

Powered by: Scopus

Follow us on @ScimagoJR

Scimago Lab, Copyright 2007-2022. Data Source: Scopus®

EST MODUS IN REBUS

Legal Notice

Privacy Policy